Revision 2: The mechanism of infiltration of metamorphic fluids recorded by hydration and carbonation of epidote-amphibolite facies metabasaltic sills in the SW Scottish Highlands

Barbara I. Kleine (corresponding author)

(barbara.kleine@geo.su.se, Tel: +46 (0)8 674 77 28, Fax: +46 (0) 8 674 78 97)

Iain K. Pitcairn

(iain.pitcairn@geo.su.se, Tel: +46 (0)8 674 7838, Fax: +46 (0) 8 674 78 97)

Alasdair D.L. Skelton

(alasdair.skelton@geo.su.se, Tel: + 46 (0)8 16 4750, Fax: +46 (0) 8 674 78 97)

Department of Geological Sciences, Stockholm University, 106 91 Stockholm, Sweden

Abstract

In this study we investigate a group of metabasaltic sills from the SW Scottish Highlands metamorphosed at epidote-amphibolite facies conditions that provide useful insight into the mechanisms and characteristics of fluid infiltration during metamorphism. The sills are amphibole and garnet bearing and exhibit a strong foliation in the sill margins that developed pre- to syn- peak metamorphism. Fluid infiltration caused hydration and carbonation in the sills, expressed as 1) replacement of garnet and amphibole by chlorite and calcite and 2) replacement of amphibole and epidote to form chlorite and calcite. Using garnet-amphibole and garnet-chlorite geothermometers we show that these reactions occurred after peak metamorphism at T = 290 to 400°C. Reaction textures show that the fluid infiltration into the sill that caused hydration and carbonation occurred in the absence of deformation. The fluid infiltration was mineralogically controlled with greater fluid access in areas of abundant fine-grained elongate minerals such as amphibole and chlorite. The replacement of garnet by

chlorite most likely occurred by an interface-coupled dissolution-precipitation mechanism as evidenced by perfect pseudomorphic textures of garnet, porosity generation behind the reactive interface and fracturing ahead of this interface. Porosity generated in the product chlorite enhanced fluid access to the replacement front. The study shows that deformation was not required for extensive fluid infiltration and alteration during metamorphism. Fluid flow uses a pre-existing foliation to gain access to the rock, taking advantage of the anisotropic shape of the aligned minerals.

Keywords

Hydration; carbonation; deformation; metamorphic fluid flow; epidote-amphibolite facies metamorphism; fluid infiltration mechanisms

Introduction

The flow of metamorphic fluids has interested geologists because of its influence on the petrological, geochemical and mechanical behavior of the Earth's crust and as a contributory factor in global chemical cycles (e.g. Bickle and McKenzie 1987; Ague 1994a, 1994b, 2003; Ferry 1994; Oliver 1996; Cartwright 1997; Ferry and Gerdes 1998). Understanding these processes relies on robust estimates of time-integrated fluid fluxes and moreover, of fluid flux rates. These estimates require an understanding of coupling between porosity-permeability evolution and metamorphic fluid flow (see review of Ague 2003 and references therein). Fluid flow in metamorphic rocks requires an interconnected porosity, either intrinsic to the rock or created during deformation. An existing pore network in the unaltered rock would significantly ease the access of external fluids and increase rates of alteration and weathering (e.g. Putnis and Mauthe 2001; Jamtveit et al. 2011, 2014). The intrinsic permeability of metamorphic rocks is strongly mineralogically controlled (e.g. Holness and Graham 1991, 1995; Ferry et al. 2005, 2013). Experimental and field studies show that monomineralic solid aggregates (e.g. marbles, quartzites) do not have a stable interconnected fluid-filled network

due to high fluid-mineral dihedral angles at certain P-T conditions (Watson and Brenan 1987; Holness and Graham 1991, 1995; Holness 1993; Price et al. 2004; Schumacher et al. 2008). As metamorphic rocks generally have low intrinsic porosity (e.g. Etheridge et al. 1984; Oliver 1996; Manning and Ingebritsen 1999; Ague 2003), deformation-driven fluid flow is commonly invoked. Many studies show enhanced metamorphic fluid flow along large-scale structural conduits such as faults (e.g. McCaig et al. 1995; Abart et al. 2002), shear zones (e.g. Selverstone et al. 1991; Gupta and Bickle 2004; Kleine et al. 2014), and fold axes (Skelton et al. 1995; Graham et al. 1997; Pitcairn et al. 2010). On a local scale deformation enhanced fluid flow can occur through dilatancy (volume change during deformation; Oliver 1996), or through hydrofracturing (Sibson et al. 1988; Thompson and Connolly 1992; Ague 1994b; Oliver and Bons 2001). The development of foliation fabrics as a response to deformation can also enhance fluid flow (Rumble and Spear 1983; Skelton et al. 1995; Ague 2007). Fluid infiltration in the absence of deformation may occur in contact metamorphic rocks where vertical upwardly-directed fluid flow is driven by buoyancy (Hanson 1992; Ferry, 1996).

The interaction between infiltrating fluid and the host rock strongly affects the permeability through destruction of porosity by precipitation of new mineral phases, and through creation of porosity due to mineral dissolution. Volume expansion of solid phases due to metamorphic carbonation and hydration reactions for example, might be expected to “clog” fluid pathways and thus limit continued fluid flow (Schliestedt and Matthews 1987). There is considerable evidence that fluid infiltration can continue despite fluid-driven reactions inducing a volume increase (e.g. Ferry 1996; Skelton et al. 1995, 2005; Ferry and Rumble, 1997). For example, Skelton et al. (2005) present seismic velocity evidence for propagation of a serpentinisation front to a depth of 2 km, despite a volume expansion exceeding 15%. Also, retrograde hydration of periclase marbles from the Beinn an Dubhaich contact aureole in Scotland progressed despite volume increase of up to 28% (Ferry 1996; Ferry and Rumble, 1997). This

implies that the permeability of the rock is temporally enhanced during mineral reaction (e.g. Putnis and Austrheim 2010). A potential cause of enhanced porosity is through the interface-coupled dissolution-precipitation mechanism (Putnis et al. 2005; Putnis 2009; Putnis and Austrheim 2010), whereby fluids can pass through reactive minerals and fluid access is sustained by porosity generation behind a replacement front. Austrheim et al. (2008) found strong support for this mechanism and intra-granular fluid flow in the form of perfectly pseudomorphed reactant phases, with their original outlines preserved by non-reacting inclusions. This mechanism suggests that permeability during metamorphic fluid flow could have been transiently higher than previously estimated. This would imply that fluid flux rates were higher and metamorphic timescales shorter than previously estimated.

In this study, we investigate possible mechanisms whereby carbonating fluids infiltrated a group of metabasaltic sills exposed at Loch Stornoway, on the west coast of Knapdale in the SW Scottish Highlands. These sills were metamorphosed at epidote-amphibolite facies conditions (metabasalts elsewhere in the SW Scottish Highlands were metamorphosed at greenschist facies conditions). This is useful because the sills contain abundant garnet that preserves excellent textural evidence for the mechanism of fluid-driven mineral reactions and controlling factors on fluid infiltration into these rocks. We show that pervasive fluid infiltration, hydration and carbonation of these rocks occurred in the absence of deformation. Further, we discuss the metamorphic conditions and relative timing at which fluid-rock interaction occurred.

Geological background

The rocks which crop out on the mainland part of the SW Scottish Highlands belong to the Argyll Group of the Dalradian Supergroup (figure 1; Harris and Pitcher 1975). The Argyll group comprises from bottom to top (1) variably calcareous phyllites interbedded with fine-grained psammites (Ardrishaig Phyllites), (2) coarser-grained to conglomeratic psammites

with variable amount of feldspar (Crinan Grits and Erins Quartzite), (3) basaltic lavas (Tayvallich Volcanics) and (4) an impure marble (Tayvallich Limestone). Much of this sequence has been intruded by mafic sills which are interpreted as representing part of a feeder system for the Tayvallich Volcanics (Graham 1976). This intrusive event has been dated at 595 ± 4 Ma based on U-Pb studies of magmatic zircons (Halliday et al. 1989).

Deformation of these rocks can be subdivided into primary and secondary phases, which have led to the formation of the Tay Nappe (figure 1; Roberts and Treagus 1977; Harte et al. 1984). Primary deformation (D_1 to D_2) produced (from NW to SE) the NW-facing Islay Anticline, upwards facing Tayvallich and Kilmory Bay Synclines (Loch Awe Syncline) and the SE-facing Ardrishaig Anticline. Primary deformation is associated with a penetrative axial planar foliation. Textural features of the deformation event D_3 during peak metamorphic temperatures (Harte et al. 1984) are not observed in the SW Scottish Highlands (Skelton et al. 1995). Secondary deformation (D_4) involved the collapse of the Ardrishaig Anticline, producing (from NW to SE) the Tarbert Monoform, Cowal Antiform, Ben Ledi Monoform and the synformal Aberfoyle Anticline (figure 1). Secondary deformation is locally associated with a crenulation cleavage which is axial planar to folds of bedding and primary cleavages (Roberts and Treagus 1977).

Metamorphism of these rocks was at greenschist to epidote-amphibolite facies conditions (Graham et al. 1983; Skelton et al. 1995) followed by a near-isothermal decompression (Vorhies and Ague 2011). Peak-metamorphic P-T conditions were 0.9 – 1.1 GPa and 550° – 580º C (Vorhies and Ague 2011). The garnet isograd delineates the approximate boundary between these facies (figure 1). This isograd is largely unaffected by primary folding but affected by secondary folding (Harte and Graham 1975) indicating that peak metamorphism

occurred towards the end of or shortly after primary deformation and predated secondary deformation.

At greenschist facies conditions CO_2-bearing, hydrous fluids caused carbonation of the metabasaltic sills which led to a characteristic mineral assemblage zonation with calcite-free interiors and calcite-rich margins (Harte and Graham 1975; Skelton et al. 1995). The fluid was probably close to equilibrium with the surrounding metasedimentary rocks (Skelton et al. 1995). Extensive carbonation is mostly seen in metabasalts metamorphosed at greenschist facies conditions (Skelton et al. 1995). However, in this study we show that carbonation also affected metabasalts which were metamorphosed at higher P-T conditions.

Methods

Samples were collected from a profile constructed across the largest sill of the group of sills which are exposed at Loch Stornoway (figure 2). Mineral modes were determined by standard point counting (1000 points per slide) with errors given from Van der Plas and Tobi (1965). Thereafter, several statistical assessments of factors which could control fluid access to garnets were used. First, abundances of garnets were determined using standard point counting as described above. However, because garnets were partly replaced by chlorite and/or calcite and because we were interested in their abundance before any hydration or carbonation occurred, we recounted garnet modes with replaced parts of garnet crystals also counted as garnet. Second, the size of each counted garnet was measured so as to assess if their degree of replacement was a function of their size. Third, the degree of replacement of the individual grains was determined by estimating the percentage of the remains of the garnet grain by visual judgment with preserved garnet = 0.0, partly replaced garnets = 0.5 and fully replaced garnets = 1.0. Mineral compositions were determined using JEOL JXA-8530 field emission electron microprobe (EMPA) at the Department of Earth Sciences, Uppsala University with running conditions of 15kV and 20 nA with a beam size of 0.5-10 μm. Whole

rock chemistry was determined using a Rigaku ZSX Primus II Sequential X-Ray Fluorescence (XRF) Spectrometer at the Department of Geological Sciences at Stockholm University. Quantification and accuracy were controlled by repeating analyses of the international glass reference materials BCR-2, AGV-2 and RGM-1 and the overall analytical error is < 5% of the measured values. The volatile content of all samples is measured as loss on ignition (LOI). Detailed bulk rock CO_2-contents were obtained by using the field-based method of Skelton *et al.* (1995) where a small volume of crushed sample reacted with HCl in a sealed vessel. The pressure of the released CO_2 gives a value for the CO_2-content of the sample. P-T estimates were obtained using conventional geothermobarometry and T-X_{CO2} diagrams were constructed using the computer program THEROMCALC (© Powell and Holland) with the database ds55 (Holland and Powell 1998).

Minerals and mineral chemistry

The group of sills at Loch Stornoway was metamorphosed in the epidote-amphibolite facies. They are similar in appearance to the greenschist facies metabasaltic sills which are found elsewhere in the SW Scottish Highlands, with massive, generally unfoliated interiors and commonly strongly foliated margins which are partly carbonated (Skelton et al. 1995; Arghe et al. 2011). However, because of their higher metamorphic grade, sills at Loch Stornoway exhibit a different mineral assemblage zonation. Sill interiors are primarily comprised of coarse-grained amphibole, epidote, plagioclase, biotite, garnet, quartz, minor calcite and accessory ilmenite rimmed by titanite (figure 3, table 1). Foliated sill margins contain fine-grained amphibole, epidote, chlorite, quartz, calcite, relicts of biotite and garnet as well as accessory titanite and rutile (figure 3, table 1). Reaction textures (see below) indicate that the sill has been affected by varying degrees of hydration and carbonation. Before discussing these reaction textures in detail, we will provide brief descriptions of each of the constituent minerals.

Amphibole is typical for the epidote-amphibolite facies. Its composition can be approximated as a 3:1 mixture of pargasite and actinolite, with X_{Fe} ~0.49 (table 2). In the sill interiors, amphibole occurs as randomly-oriented, coarse-grained, subhedral equant/columnar prisms (figure 4a). Crystals show blue-green pleochroism and evidence of only minimal patchy zoning. In the sill margins, amphibole occurs as subhedral, fine-grained, acicular/fibrous prisms with strong preferred orientation (figure 4b). Crystals also show blue-green pleochroism. Calcite and chlorite are seen replacing amphibole in the sill margins (figure 5a).

Epidote (X_{Cz} ~ 0.5) occurs throughout the sill as high relief subhedral grains with yellowish to purple pleochroism (figure 6a). Epidote also appears as replacement product after garnet (figure 6b). In the sill margins epidote is replaced by calcite (figure 5b).

Garnet is mostly almandine (X_{Alm} = 0.55 ± 0.04) and grossular (X_{Gross} = 0.29 ± 0.02). It contains smaller spessartine (X_{Spess} = 0.14 ± 0.03) and negligible pyrope (X_{Py} = 0.01 ± 0.01) (table 2). Garnet occurs as small euhedral crystals (0.2 – 0.6 mm) throughout the sill with highest abundance in the sill interiors (figure 7). Most of the garnets are partially or wholly replaced by chlorite (figure 2). The largest and least altered garnet crystals occur in the sill interior (figures 2 and 7b). Inclusions of quartz and epidote commonly occur in the rims of these garnets. Replacement of garnet occurs throughout the sills but is most extensive in the sill margins (figure 2). Partially replaced garnets perfectly retain their original outline with chlorite and sometimes calcite replacing garnet from the edges of the polyhedron inward (figure 2). The chlorite produced during this replacement reaction has considerably higher porosity than the garnet (figures 8a). Replacement is enhanced when the initial garnet crystal contains inclusions of quartz and/or epidote in the rims and cracks. Close to the sill margins preserved garnets are commonly surrounded by coarse-grained quartz and/ or enclosed by calcite (figures 6c,d). In a few rare cases garnet is preserved in zones of the sill that are

196 foliated but uncarbonated. In these cases small inclusions of quartz, epidote, and amphibole
197 imitate the orientation of foliation in the surrounding rock formed by alignment of amphibole
198 (figure 2f).

199 *Biotite* is slightly enriched in Fe with $X_{Fe} \sim 0.6$ (table 2). Biotite occurs as randomly-oriented
200 subhedral, coarse-grained, platy crystals with pale brown pleochroism. These are often ragged
201 in appearance, particularly near the sill margin, where biotite is replaced by calcite and
202 chlorite both at its rims and along cleavage surfaces (figure 5c).

203 *Chlorite* ($X_{Fe} \sim 0.5$; table 2) occurs as small pale green platy crystals, with an anomalous
204 purple interference color and is most abundant in the sill margins. In the sill margins, chlorite
205 occurs as matrix grains, but also replacing amphibole, garnet and biotite (figure 5). In the sill
206 interior, chlorite predominantly occurs as a replacement product of garnet (figure 2). Its
207 orientation is often controlled by the crystallography of the crystal it is replacing. This is most
208 spectacularly illustrated by its replacement of garnet, where replacement chlorites outline a
209 hexagonal pattern tracing the crystal structure of the original garnet (figure 2).

210 *Plagioclase* is almost pure albite with $X_{ab} \sim 0.99$ (table 2). It mostly occurs as anhedral grains
211 filling interstices between other mineral grains. Relic phenocrysts are most easily seen in the
212 field. In thin section, such relics are largely obscured by replacement to epidote.

213 *Quartz* occurs as small equant grains throughout the sills. Its abundance is greatest near the
214 sill margins. Coarser-grained quartz is seen surrounding garnets which have not been
215 replaced.

216 *Calcite* occurs as replacement product after biotite, epidote, amphibole and garnet (figure 5)
217 where it grows along cleavages and cracks in the reactant minerals (figure 8b). Calcite also
218 occurs in coarser grained patches (figure 4c). Higher abundances of calcite are restricted to

the sill margins (figure 3, table 1) with the exception of the sample taken at 49.3 m. The high calcite content of this sample might relate to bifurcation of the sill (figure 2).

Pressure-temperature conditions of alteration

The metabasalt at Loch Stornoway contains mineral pairs that are useful for constraining metamorphic temperatures. These include garnet-amphibole and garnet-chlorite. Because coexistence of garnet and amphibole is characteristic of the epidote-amphibolite facies in Fe-rich metabasalts (Spear 1993) and because textural evidence confirms that garnet replacement by chlorite occurred in response to carbonation and hydration, we can use garnet-hornblende and garnet-chlorite geothermometers to constrain the timing of fluid-rock interaction with respect to the P-T evolution of the SW Scottish Highlands.

Metamorphic temperatures were calculated based on rim-rim mineral pairs for both garnet-amphibole and garnet-chlorite for an assumed metamorphic pressure of 1 GPa, which was obtained using the phengite geobarometer by Skelton et al. (1995) and which is also in agreement with Vorhies and Ague (2011). For the garnet-amphibole geothermometer, we compared temperatures estimated using the calibrations by Graham and Powell (1984) and Ravna (2000) (table 3), and for the garnet-chlorite geothermometer, we compare temperatures estimated using the calibrations of Dickenson and Hewitt (1986), Ghent et al. (1987), Perchuk (1981) and Grambling (1990) (table 4). The two calibrations of the garnet-amphibole geothermometer (table 3) yielded temperatures ranging from 380 to 470°C (mean 425°C). The six calibrations of the garnet-chlorite geothermometer (table 4) yielded temperatures ranging from 290 to 400°C (mean 340°C). We add a cautionary note that our interpreted mechanism for garnet replacement (see below) might preclude garnet-chlorite equilibrium. However, temperatures obtained using this thermometer, are slightly lower than those

obtained using garnet-hornblende geothermometry, which might be expected if chlorite replaced garnet during retrograde metamorphism.

Whole rock chemistry

Whole rock chemical data from the profile sampled across the largest metabasaltic sill at Loch Stornoway (figure 2) with oxides reported as wt% on a volatile free basis are listed in table 5 and shown graphically in figure 9. Concentrations of major elements that are discussed hereafter in the text are averaged concentrations (± 1 s.d.) from the profile (table 5) if not otherwise stated.

Concentrations of Al_2O_3 (13.1 ± 0.4 wt%), MgO (5.2 ± 0.3 wt%), MnO (0.2 ± 0.03 wt%) and P_2O_5 (0.2 ± 0.04 wt%) show only minor variation throughout the sill. Concentrations of Fe_2O_3 (18.1 to 20.2 wt%) and TiO_2 (3.7 to 4.3 wt%) are highest in the eastern sill margin with lower values in the sill interior (15.9 ± 1.1 wt% for Fe_2O_3 and 2.7 ± 1.5 wt% for TiO_2). Concentrations of Na_2O tend to be higher in the sill interior (2.3 ± 0.3 wt%) than in the sill margins (1.4 ± 0.5 wt%). Concentrations of CaO are lowest in the western sill margin (7.7 ± 0.04 wt%) in comparison to the rest of the sill (9.1 ± 0.5 wt%). K_2O varies strongly throughout the sill with highest concentration values in the western and lowest concentration values in the eastern sill margin. The volatile content which was measured as loss on ignition (LOI), with systematically higher values of 6.6 ± 0.1 wt% occurring in the sill margins compared to the sill interior (1.2 ± 0.6 wt%).

Hydration and carbonation reactions in the Loch Stornoway sills

Textural evidence of both hydration and carbonation are seen at Loch Stornoway. Replacement of amphibole and epidote by calcite and chlorite occurs in the sill margins (figure 5a,b), as has been reported in previous studies of greenschist facies metabasaltic sills from the same area (Graham et al. 1983; Skelton et al. 1995). Replacement of garnet by

chlorite and minor amounts of calcite is seen at various stages of completion throughout each of the sills (figures 2 and 5d). In general, replacement of garnets is more extensive closer to the sill margins, but even in the interior of the largest sill, most garnets are at least partially replaced by chlorite and sometimes calcite. Throughout the sills, partially and wholly replaced garnets are perfectly pseudomorphed, with their initial outline preserved (figure 2). This has been observed both in foliated and non-foliated parts of the metabasaltic sills. Of importance, the chlorite that replaces the garnet does not show any preferred orientation even in foliated parts of the sills. Instead, chlorite growth is crystallographically controlled with respect to the former outline of the garnets (figure 2). Also, calcite replacing garnet grows as almost perfect rhomboidal crystals within the former outline of the garnet (figure 5d). This implies that the replacement of garnet by chlorite and calcite occurred under low strain conditions. Another texture observed is the replacement of biotite by chlorite and calcite (figure 5a,c). As is also the case for amphibole, growth of chlorite and calcite is crystallographically controlled by the reactant mineral forming along cleavage planes and preserving the original outline of reactant minerals.

The computer program THERMOCALC was used together with mineral chemistry (table 2), and modal variations estimated by point counting (figure 3, table 1) to identify probable reactions responsible for the observed reaction textures. Mineral endmember activities were calculated from microprobe data (table 2) by using the software AX (© Holland 2008). In this analysis, we identified the following reactions that could have caused replacement of garnet, amphibole and epidote by chlorite and calcite:

$$25\ \underset{Fe_3Al_2Si_3O_{12}}{\text{almandine}} + 4\ \underset{Ca_2Fe_5Si_8O_{22}(OH)_2}{\text{ferroactinolite}} + 74\ H_2O = 19\ \underset{Fe_5Al_2Si_3O_{10}(OH)_4}{\text{daphnite}} + 4\ \underset{Ca_2Al_3Si_3O_{12}(OH)}{\text{clinozoisite}} + 38\ \text{quartz} \quad (1)$$

$$5\ \underset{Fe_3Al_2Si_3O_{12}}{\text{almandine}} + 2\ \underset{Ca_2Fe_5Si_8O_{22}(OH)_2}{\text{ferroactinolite}} + 4\ CO_2 + 18\ H_2O = 5\ \underset{Fe_5Al_2Si_3O_{10}(OH)_4}{\text{daphnite}} + 16\ \text{quartz} + 4\ \text{calcite} \quad (2)$$

291 3 ferroactinolite + 2 clinozoisite + 10 CO_2 + 8 H_2O= 3 daphnite + 10 calcite + 21 quartz (3)
292 $Ca_2Fe_5Si_8O_{22}(OH)_2$ $Ca_2Al_3Si_3O_{12}(OH)$ $Fe_5Al_2Si_3O_{10}(OH)_4$

293 Reactions (1) and (2) could explain partial replacement of garnet by chlorite or chlorite and
294 calcite throughout the sill, whereas reaction (3), which is the Fe-endmember version of the
295 reaction suggested to occur at greenschist facies conditions in other carbonated sill margins in
296 the SW Highlands (Skelton et al. 1995), could explain replacement of amphibole and epidote
297 in the sill margins. Reactions (1), (2) and (3) are isochemical with respect to non-volatiles and
298 are supported by textural and modal data (figures 3, 5 and 6b). One reaction texture not
299 explained by these reactions is replacement of biotite by chlorite and calcite (figure 5c).
300 Biotite is the only major K-bearing mineral in the metabasaltic sills as shown by the positive
301 correlation between the abundance of biotite and the concentration of K_2O (figure 10). As
302 there is no product mineral for the K mobilized by breakdown of biotite we suggest that K
303 was removed by the carbonating fluid. Another possibility is that biotite mode reflects a pre-
304 metamorphic gradient in the K_2O-content of the sill and biotite crystals provide preferred
305 nucleation sites for chlorite and calcite produced by reactions (2) and/ or (3).

306 **Fluid composition**

307 Reactions (1-3) can be represented on a T-X_{CO2} diagram (figure 11). Use of this diagram
308 assumes that the fluid is a binary mixture of H_2O and CO_2. This is consistent with reaction
309 textures that show intergrown calcite and chlorite replacing garnets (figure 5d) and calcite
310 surrounding and sealing off fresh garnets in the sill margins (figure 6d). The reactions plotted
311 on this T-X_{CO2} diagram include only Fe-endmembers. Involving Mg in the calculations
312 performed by THERMOCALC results in a shift of the junction of the three reactions towards
313 lower X_{CO2} and T. The topology, however, remains unchanged. For the purpose of this study,
314 the Fe-endmembers are sufficient to illustrate the process of fluid front propagation. Skelton
315 et al. (1995) argued that the carbonating fluid was sourced from the metapelitic rocks which
316 host the metabasalts. The metapelites contain the mineral assemblage: chlorite + rutile +

calcite + quartz + albite. This assemblage buffers X_{CO2} to 0.002 – 0.003 for the temperature range 290 to 400°C (Skelton et al. 1995).

In the following section, we will discuss two possible reaction pathways which might explain fluid front propagation at Loch Stornoway. Both reaction pathways assume that the fluid composition was buffered at X_{CO2} = 0.002 – 0.003 (figure 11). The first reaction pathway assumes that infiltration of an externally-buffered fluid occurred as temperature was decreasing (blue arrow, figure 11a) causing separate hydration and carbonation. Hydration of garnet and amphibole (reaction 1) would occur first, and as temperatures decrease the infiltrating fluid will eventually cause carbonation of the remaining amphibole and epidote (reaction 3). The occurrence of purely hydrated garnet in the sill interior supports this mechanism (figure 6b). However, this reaction pathway does not explain the occurrence of both hydrated and carbonated garnets.

The second reaction pathway invokes two separate carbonation reactions occurring simultaneously within the temperature range given by garnet-chlorite geothermometry (290 to 400°C, red box). Within this temperature range carbonation of garnet and amphibole (reaction 2) and carbonation of amphibole and epidote (reaction 3) can be driven simultaneously by infiltration of a fluid with X_{CO2} greater than that which is buffered by reaction 3 and less than that which is buffered by the reaction 2 (figure 11b).

Propagation of reaction fronts

For reaction pathway 2, a comparison of the distance of reaction fronts for the two reactions 2 and 3 driven by the same fluid flux perpendicular to the sill contact can explain the variations in garnet replacement textures across the entire sill while carbonation of amphibole and epidote was restricted to the margins. For a simple transport model that ignores diffusion and kinetic broadening, we can consider advective displacement of reaction fronts associated with

reactions 2 and 3 from the western margin of the main sill. This is based on the slight asymmetry of its calcite content distribution in the western sill margin at 0.7 m (14.7 ± 2.2 vol%) compared to the calcite content in the western sill margin at 73.9 m (10.8 ± 2.0 vol%) along the profile (figure 3). We note, however that carbonation of both sill margins implies that front displacement is partly due to diffusion. For a fluid composition of X_{CO2} = 0.002 – 0.003 we can estimate the front displacement (*Z*) for reactions (2) (carbonation of garnet) and (3) (carbonation of amphibole and epidote) relative to one another for pure advection, by solving the following equation (Skelton et al. 1995) for both reactions simultaneously with time-integrated fluid flux (q_m) fixed:

$$q_m = Z * \frac{N_{CO2} - X_{CO2,final} * (N_{CO2} + N_{H2O})}{X_{CO2,final} - X_{CO2,initial}} \quad \text{(eq. 1)}$$

where $X_{CO2,intial}$ and $X_{CO2,final}$ are fluid compositions upstream and downstream of each reaction front, and N_{CO2} and N_{H2O} are the number of moles of CO_2 and H_2O produced (+) or consumed (-) by each reaction per cubic meter of rock. $X_{CO2,initial}$ is 0.002 - 0.003 from Skelton et al. (1995) and $X_{CO2,final}$ for each reaction can be read from figure 11 for a temperature range of 290 – 400°C. N_{CO2} and N_{H2O} for each reaction is calculated from the stoichiometric coefficients for H_2O and CO_2 and the molar proportions of calcite in the rock after each reaction according to the method of Skelton et al. (1995). As q_m is same for reactions (2) and (3), we can equalize the second part of equation (1) for both reactions and solve for the ratio of front displacement. We estimate that the reaction front for reaction (2) will propagate 1020 – 1230 times further than the reaction front of reaction (3). Given a front displacement of ca. 1 m for carbonation of amphibole and epidote (reaction 3) (figure 11), we estimate a front displacement of ca 1 km for carbonation of garnet (reaction 2). This explains why carbonation of garnet occurs throughout the sill (figure 7b). Reaction progress in the sill interior was however incomplete with many fresh and partially replaced garnets and low

365 calcite modes. Reactions 2 and 3 involve CO_2 and H_2O as reactants and can be classified as
366 carbonation-hydration reactions. The occurrence of calcite is patchy in the sill interior (figures
367 3, 7b). This could reflect hydration of garnets in one part of the sill and precipitation of calcite
368 elsewhere.

369 The reaction textures show that irrespective of which reaction pathway is favored, carbonation
370 was unassisted by deformation as the former outlines of garnets are still preserved, even in the
371 sill margins. This would not have been the case if carbonation was accompanied by
372 deformation as it is suggested by Skelton et al. (1995). On the basis of the textural evidence
373 and the composition of chlorite we favor the second reaction pathway, but in terms of
374 understanding the mechanisms of fluid infiltration and mineral replacement, it does not really
375 matter which of the reaction pathways occurred.

376 **Mechanism of mineral replacement**

377 Reactions (1-3) yield an overall volume expansion of the solid phases for each reaction. The
378 calculated volume changes are approximately +9 % for reaction (1), +14 % for reaction (2)
379 and +19% for reaction (3), based on mineral compositions given in table 2. The direct
380 replacement of garnet by chlorite involves a density reduction from 4.00 ± 0.01 to 2.95 ± 0.01
381 $g.cm^{-3}$ (table 2). This equates to a volume expansion of ~35 %. No evidence of this volume
382 change such as disruption of original grain shapes is observed within the garnets, but as more
383 than one reactant phase is involved in all of these reactions, it is possible that volume gain
384 could occur outside the garnet crystal, e.g. in the foliated parts of the sill. However, as the
385 metabasaltic sills are not strongly altered this volume change would be negligible. Partial or
386 total replacement of garnet by chlorite with near-perfect preservation of the original garnet
387 grain outlines suggests that at the scale of individual crystals (< 1 mm), replacement did not
388 involve a change of volume and must therefore have been coupled with some mobility of non-

389 volatile components. For example, constant volume replacement of garnet by chlorite could
390 occur by the reaction (cf. Putnis 2009):

391 $1.00\ \underset{Fe_3Al_2Si_3O_{12}}{\text{almandine}} + 1.08\ H_2O + 5.53\ H^+ = 0.54\ \underset{Fe_5Al_2Si_3O_{10}(OH)_4}{\text{daphnite}} + 1.38\ H_4SiO_4 + 0.92\ Al^{3+} + 0.30\ Fe^{2+}$
392
393

394 with molar volumes of the Fe-endmembers of garnet and chlorite taken from Holland and
395 Powell (1998). Reaction (4) liberates Si, Al and Fe that are probably taken up by
396 crystallization of quartz, chlorite and epidote elsewhere (figures 5d, 6b). This observation is
397 consistent with replacement having occurred by interface-coupled dissolution and
398 precipitation (e.g. Putnis and Austrheim 2010). This mechanism has been shown to sustain
399 pathways between the fluid source (outside the reactant crystal) and the replacement front as
400 it advances into the reactant crystal (Putnis 2009). This not only permits fluid access to the
401 replacement front but also provides pathways for addition or removal of other (non-fluid)
402 components. In the cases of garnet replacement by chlorite, epidote and calcite in this study,
403 removal of primarily SiO_2 from the reactant crystals along such pathways is likely to (1)
404 maintain near constant volume and (2) explain the absence of quartz as a product phase in
405 replacement textures. The whole rock chemical data (table 5; figure 9) suggest that on a hand-
406 specimen scale, the progress of these reactions is isochemical with respect to the solid
407 components (with the possible exception of the carbonation of biotite that would release K)
408 and that the only components that are added to the rock are H_2O and CO_2. The bulk
409 composition of the metabasalt remains constant because SiO_2 that is removed from these
410 replacement fronts is precipitated nearby as quartz (e.g. figure 6b). This observation is similar
411 to that of Carmichael (1969) for the transformation of kyanite to sillimanite and provides
412 evidence that reactions (1) and (2) are metasomatic at the scale of individual crystals (<1 mm)
413 while they are isochemical at the scale of a hand specimen (>5–10 cm).

Mechanisms of fluid infiltration

The sill margins are extensively affected by carbonation and hydration. Garnets are almost completely replaced by chlorite and calcite. Modes of amphibole decrease significantly in the sill margins where calcite modes are higher. The extent of foliation in the margins strongly correlates with the degree of carbonation. The relationship occurs throughout the sills in the SW Highlands and has been interpreted to indicate that the foliation developed during the carbonation event (Skelton et al. 1995, 1997; Arghe et al. 2011). However, the higher metamorphic grade of the sills at Loch Stornoway allows us to re-evaluate the timing of foliation development and influence of deformation on fluid infiltration. At Loch Stornoway we observe foliated zones of the sill that are not affected by carbonation. In these zones the foliation is controlled by alignment of amphibole (figure 4). Garnet within these zones also preserved the foliation through alignment of mineral inclusions (figure 2). This implies that the foliation in the sill margins developed during prograde to peak metamorphism. This is in agreement with previous workers who suggest garnet growth and peak metamorphic conditions occurred somewhere between the D_2 and D_3 deformation events (Harte et al. 1984; McLellan 1985; Vorhies and Ague 2011). Replacement of the garnets must have occurred after their formation at peak metamorphic conditions. Based on these observations and the temperature estimates derived from geothermometry, we conclude that chlorite rims formed after peak (epidote-amphibolite facies) metamorphism. This is consistent with textural observations showing that garnet growth occurred syn-tectonically while hydration and carbonation of garnets occurred after deformation (figure 2).

The replaced garnets still preserve their original outline, and new growth of chlorite was crystallographically controlled with no indication of a stress regime causing preferential orientation of the chlorite (figure 2). This is also supported by calcite growth in a nearly perfect rhomboidal shape within the former garnet (figure 5d). These observations imply that

fluid infiltration into the metabasalt occurred in a period of low differential stress, unassisted by deformation. The fluid most likely exploited the pre-existing foliation in the metabasaltic sill margins but the occurrence of hydrated and carbonated garnets throughout the sill indicate that fluid infiltration was not critically hindered by the lack of foliation in the sill interior. In some samples from the sill interior, fully and partially replaced garnets can occur together with pristine garnets. Examination of the bordering mineral grains of these garnets reveals that partially and fully replaced garnets are commonly surrounded by chlorite, amphibole and epidote, whereas the fresh garnets are commonly surrounded by coarse-grained quartz, albite and/ or calcite (figure 6c,d). These minerals may seal off the individual garnet grains from infiltrating fluid thus inhibiting the progression of hydration and carbonation reactions. High dihedral angles between fluid and crystals have been shown to inhibit fluid ingress in monomineralic solids composed of calcite or quartz (Watson and Brenan 1987; Holness and Graham 1991; Holness 1993; Price et al. 2004), and a similar process may explain sealing of preserved garnet grains in these sills. Another interesting relationship is the grain size of amphibole (figure 4a,b) and degree of replacement of the garnets (figure 7b). Amphibole is usually coarse grained in areas with high abundance of fresh garnets (sill interior). In areas where garnets are dominantly replaced, the grain size of amphibole decreases. These observations point to a control on fluid infiltration and the extent of hydration reactions in the sill interiors. Larger grain sizes and/or zones of monomineralic calcite, albite or calcite appear to restrict fluid flow. This leads to the interpretation that fluids will preferentially gain access into the sill interior along boundaries of elongated or platy, fine-grained minerals such as amphibole and chlorite. The creation of porosity through the interface-coupled dissolution precipitation mechanism (figure 8a) contributed to fluid infiltration, but the extent to which this mechanism promoted fluid access to the entire sill rather than just the hydration fronts in garnet grains, is not clear. In the sill margins fluid flow was most likely enhanced both by the

abundance of fine-grained elongate/ platy minerals and the occurrence of a pre-existing foliation. Fluid infiltration into the sill may have been driven by the reduction of surface free energy due to wetting of grain boundaries (cf. Spencer 1981).

Implications for metamorphic fluid flow in the SW Scottish Highlands

Carbonation and hydration reactions in garnet bearing metabasaltic sills at Loch Stornoway in the SW Highlands of Scotland provide insight into mechanisms of fluid flow and alteration during metamorphism and allow re-evaluation of the timing and driving forces for fluid flow in the SW Highlands (figure 12). Reaction textures show that the infiltration of H_2O-CO_2 fluid occurred in the absence of deformation, as is spectacularly demonstrated by pseudomorphic replacement of garnet by chlorite. The foliation of the sill margins clearly developed contemporaneously with garnet growth during prograde to peak metamorphism, prior to alteration. The sequence of events as indicated from the sills in this study are 1) development of foliation during prograde to peak metamorphism on the margins of the sills. This most likely formed during either D_1 or D_2 and was contemporaneous with garnet growth at peak metamorphic temperatures > 425°C. 2) Infiltration of H_2O-CO_2 fluid along grain boundaries of platy minerals such as amphibole. This occurred after peak metamorphism at temperatures of around 340°C.

Deformation is commonly invoked for allowing fluid access during metamorphism, particularly during the retrograde part of the metamorphic cycle (e.g. Yardley et al. 2000). The textural observations at Loch Stornoway provide an example of fluid infiltration and retrograde alteration in the absence of significant deformation. Fluid flow uses a pre-existing foliation, thereby only taking advantage of mineral anisotropy to allow fluid access into the metabasaltic sills.

In other words, previous deformation causes a mineralogical control on fluid flow. As such, the focusing of fluid flow in antiformal fold axes in the SW Scottish Highlands (Skelton et al. 1995; Pitcairn et al. 2010) should be considered as mineralogically controlled. Alignment of the minerals was controlled by deformation but flow of the fluid, which occurred considerably later, was controlled by the mineral orientations. This sequence of events has not been previously observed due to the similarity in mineralogy of prograde and alteration induced assemblages formed at greenschist facies conditions. It is only through investigation of higher metamorphic grade sills that it has been possible to show that foliation developed during prograde metamorphism but carbonation and hydration occurred during retrograde metamorphism in the absence of deformation. We also suggest that the timing of fluid flow and alteration we describe in this study applies to the other studies in the SW Scottish Highlands.

Acknowledgements

This work has been financially supported by the EU Initial Training Network Delta-Min (Mechanisms of Mineral Replacement Reactions) grant and the Navarino Environmental Observatory (NEO), Messinia, Greece, a cooperation between Stockholm University, the Academy of Athens and TEMES S.A.. XRF analyses were generated at the lab facilities of the Department of Geological Sciences, Stockholm University, which are partially supported by the Knut & Alice Wallenberg Foundation. The authors would like to thank M. Ahlbom, H. Harrysson, R. Jacobson and D. Zetterberg for their contribution during sample preparation and analyses. J. Ferry and an anonymous reviewer are thanked for their helpful and constructive reviews. The authors also would like to thank S. Penniston-Dorland for careful and thoughtful editorial handling of this study.

References cited

Abart, R., Badertscher, N., Burkhard, M., and Povoden, E. (2002) Oxygen, carbon and strontium isotope systematics in two profiles across the Glarus thrust: implications for fluid flow. Contributions to Mineralogy and Petrology, 143, 192-208.

Ague, J.J. (1994a) Mass transfer during Barrovian metamorphism of pelites, south-central Connecticut; I, Evidence for changes in composition and volume. American Journal of Science, 294, 989-1057.

Ague, J.J. (1994b) Mass transfer during Barrovian metamorphism of pelites, south-central Connecticut; II, Channelized fluid flow and the growth of staurolite and kyanite. American Journal of Science, 294, 1061-1134.

Ague, J.J. (2003) Fluid flow in the deep crust. Treatise on geochemistry, 3, 195-228.

Ague, J.J. (2007) Models of permeability contrasts in subduction zone mélange: implications for gradients in fluid fluxes, Syros and Tinos Islands, Greece. Chemical Geology, 239, 217-227.

Arghe, F., Skelton, A.D.L., and Pitcairn, I.K. (2011) Spatial coupling between spilitization and carbonation of basaltic sills in SW Scottish Highlands: evidence of a mineralogical control of metamorphic fluid flow. Geofluids, 11, 245-259.

Austrheim, H., Putnis, C.V., Engvik, A.K., and Putnis, A. (2008) Zircon coronas around Fe–Ti oxides: a physical reference frame for metamorphic and metasomatic reactions. Contributions to Mineralogy and Petrology, 156, 517-527.

Bickle, M.J., and McKenzie, D. (1987) The transport of heat and matter by fluids during metamorphism. Contributions to Mineralogy and Petrology, 95, 384-392.

Carmichael, D.M. (1969) On the mechanism of prograde metamorphic reactions in quartz-bearing pelitic rocks. Contributions to Mineralogy and Petrology, 20, 244-267.

Cartwright, I. (1997) Permeability generation and resetting of tracers during metamorphic fluid flow: implications for advection-dispersion models. Contributions to Mineralogy and Petrology, 129, 198-208.

Dickenson, M.P., and Hewitt, D.A. (1986) A garnet-chlorite geothermometer. Abstracts with Programs - Geological Society of America, 18, 584.

Etheridge, M.A., Wall, V.J., Cox, S.F., and Vernon, R.H. (1984) High fluid pressures during regional metamorphism and deformation: implications for mass transport and deformation mechanisms. Journal of Geophysical Research: Solid Earth (1978–2012), 89, 4344-4358.

Ferry, J.M. (1994) Role of fluid flow in the contact metamorphism of siliceous dolomitic limestones. American Mineralogist, 79, 719-736.

Ferry, J.M. (1996) Prograde and retrograde fluid flow during contact metamorphism of siliceous carbonate rocks from the Ballachulish aureole, Scotland. Contributions to Mineralogy and Petrology, 124, 235-254.

Ferry, J.M. and Rumble III, D. (1997) Formation and destruction of periclase by fluid flow in two contact aureoles. Contributions to Mineralogy and Petrology, 128, 313-334.

Ferry, J.M., and Gerdes, M.L. (1998) Chemically reactive fluid flow during metamorphism. Annual Review of Earth and Planetary Sciences, 26, 255-287.

Ferry, J.M., Rumble III, D., Wing, B.A., and Penniston-Dorland, S.C. (2005) A new interpretation of centimeter-scale variations in the progress of infiltration-driven metamorphic

553 reactions: case study of carbonated metaperiodite, Val d'Efra, Central Alps, Switzerland.
554 Journal of Petrology, 46, 1725-1746.

555 Ferry, J.M., Winslow, N.W., and Penniston-Dorland, S.C. (2013) Re-evaluation of
556 Infiltration-driven Regional Metamorphism in Northern New England: New Transport
557 Models with Solid Solution and Cross-layer Equilibration of Fluid Composition. Journal of
558 Petrology, 54, 2455-2485.

559 Ghent, E.D., Stout, M.Z., Black, P.M., and Brothers, R.N. (1987) Chloritoid-bearing rocks
560 associated with blueschists and eclogites, northern New Caledonia. Journal of Metamorphic
561 Geology, 5, 239-254.

562 Graham, C.M. (1976) Petrochemistry and tectonic significance of Dalradian metabasaltic
563 rocks of the SW. Scottish Highlands. Journal of the Geological Society, 132, 61-84.

564 Graham, C.M., and Powell, R. (1984) A garnet–hornblende geothermometer: calibration,
565 testing, and application to the Pelona Schist, Southern California. Journal of metamorphic
566 Geology, 2, 13-31.

567 Graham, C.M., Greig, K.M., Sheppard, S.M.F., and Turi, B. (1983) Genesis and mobility of
568 the H_2O-CO_2 fluid phase during regional greenschist and epidote amphibolite facies
569 metamorphism: a petrological and stable isotope study in the Scottish Dalradian. Journal of
570 the Geological Society, 140, 577-599.

571 Graham, C.M., Skelton, A.D.L., Bickle, M.J., and Cole, C. (1997) Lithological, structural and
572 deformation controls on fluid flow during regional metamorphism. Mineralogical Society
573 Series, 8, 196-226.

574 Grambling, J.A. (1990) Internally-consistent geothermometry and H_2O barometry in
575 metamorphic rocks: the example garnet-chlorite-quartz. Contributions to Mineralogy and
576 Petrology, 105, 617-628.

577 Gupta, S., and Bickle, M.J. (2004) Ductile shearing, hydrous fluid channelling and high-
578 pressure metamorphism along the basement-cover contact on Sikinos, Cyclades, Greece.
579 Geological Society, London, Special Publications, 224, 161-175.

580 Halliday, A.N., Graham, C.M., Aftalion, M., and Dymoke, P. (1989) Short Paper: The
581 depositional age of the Dalradian Supergroup: U-Pb and Sm-Nd isotopic studies of the
582 Tayvallich Volcanics, Scotland. Journal of the Geological Society, 146, 3-6.

583 Hanson, R.B. (1992) Effects of fluid production on fluid flow during regional and contact
584 metamorphism. Journal of Matamorphic Geology 10, 87-97.

585 Harris, A.L., and Pitcher, W. (1975) The Dalradian Supergroup - A Correlation of the
586 Precambrian Rocks of the British Isles. Geological Society, London, Special Reports, 6, 52-
587 75.

588 Harte, B., and Graham, C.M. (1975) The graphical analysis of greenschist to amphibolite
589 facies mineral assemblages in metabasites. Journal of Petrology, 16, 347-370.

590 Harte, B., Booth, J.E., Dempster, T.J., Fettes, D.J., Mendum, J.R., and Watts, D. (1984)
591 Aspects of the post-depositional evolution of Dalradian and Highland Border Complex rocks
592 in the Southern Highlands of Scotland. Transactions of the Royal Society of Edinburgh: Earth
593 Sciences, 75, 151-163.

594 Holland, T.J.B., and Powell, R. (1998) An internally consistent thermodynamic data set for
595 phases of petrological interest. Journal of metamorphic Geology, 16, 309-343.

Holness, M.B. (1993) Temperature and pressure dependence of quartz-aqueous fluid dihedral angles: the control of adsorbed H_2O on the permeability of quartzites. Earth and Planetary Science Letters, 117, 363-377.

Holness, M.B., and Graham, C.M. (1991) Equilibrium dihedral angles in the system H_2O-CO_2-NaCl-calcite, and implications for fluid flow during metamorphism. Contributions to Mineralogy and Petrology, 108, 368-383.

Holness, M.B., and Graham, C.M. (1995) PTX effects on equilibrium carbonate-H_2O-CO_2-NaCl dihedral angles: constraints on carbonate permeability and the role of deformation during fluid infiltration. Contributions to Mineralogy and Petrology, 119, 301-313.

Jamtveit, B., Kobchenko, M., Austrheim, H., Malthe-Sørenssen, Røyne, A. and Svensen, H. (2011). Porosity evolution and crystallization-driven fragmentation during weathering. Journal of Geophysical Research 116, doi:10.1029/2011JB008649.

Jamtveit, B., Krotkiewski, M., Kobchenko, M., Renard, F. and Angheluta, L. (2014) Pore-space distribution and transport properties of an andesitic intrusion. Earth and Planetary Science Letters, 400, 123 -129.

Kleine, B.I., Skelton, A.D.L., Huet, B., and Pitcairn, I.K. (2014) Preservation of Blueschist-facies Minerals along a Shear Zone by Coupled Metasomatism and Fast-flowing CO_2-bearing Fluids. Journal of Petrology, 55, 1905-1939.

Manning, C.E., and Ingebritsen, S.E. (1999) Permeability of the continental crust: Implications of geothermal data and metamorphic systems. Reviews of Geophysics, 37, 127-150.

McCaig, A.M., Wayne, D.M., Marshall, J.D., Banks, D., and Henderson, I. (1995) Isotopic and fluid inclusion studies of fluid movement along the Gavarnie Thrust, central Pyrenees; reaction fronts in carbonate mylonites. American Journal of Science, 295, 309-343.

McLellan, E. (1985) Metamorphic reactions in the kyanite and sillimanite zones of the Barrovian type area. Journal of Petrology, 26, 789-818.

Oliver, N.H.S. (1996) Review and classification of structural controls on fluid flow during regional metamorphism. Journal of Metamorphic Geology, 14, 477-492.

Oliver, N.H.S., and Bons, P.D. (2001) Mechanisms of fluid flow and fluid–rock interaction in fossil metamorphic hydrothermal systems inferred from vein–wallrock patterns, geometry and microstructure. Geofluids, 1, 137-162.

Perchuk, L.L. (1981) Correction of biotite-garnet thermometer for the case of Mn reverseble Mg+ Fe isomorphism in garnet. Doklady Akademii Nauk SSSR, 256, 441-442.

Pitcairn, I.K., Skelton, A.D.L., Broman, C., Arghe, F., and Boyce, A. (2010) Structurally focused fluid flow during orogenesis: the Islay Anticline, SW Highlands, Scotland. Journal of the Geological Society, 167, 659-674.

Price, J.D., Wark, D.A., and Watson, B.E. (2004) Grain-scale permeabilities of synthetic quartzite with volumetrically minor phlogopite, corundum, or aluminosilicate. Earth and Planetary Science Letters, 227, 491-504.

Putnis, A. (2009) Mineral replacement reactions. Reviews in mineralogy and geochemistry, 70, 87-124.

Putnis, A. and Mauthe, G. (2001) The effect of pore size on cementation in porous rocks. Geofluids, 1, 37-41.

639 Putnis, A., and Austrheim, H. (2010) Fluid-induced processes: metasomatism and
640 metamorphism. Geofluids, 10, 254-269.

641 Putnis, C.V., Tsukamoto, K., and Nishimura, Y. (2005) Direct observations of
642 pseudomorphism: compositional and textural evolution at a fluid-solid interface. American
643 Mineralogist, 90, 1909-1912.

644 Ravna, E.K. (2000) Distribution of Fe2+ and Mg between coexisting garnet and hornblende in
645 synthetic and natural systems: an empirical calibration of the garnet-hornblende Fe-Mg
646 geothermometer. Lithos, 53, 265-277.

647 Roberts, J.L. (1974) The structure of the Dalradian rocks in the SW Highlands of Scotland.
648 Journal of the Geological Society, 130, 93-124.

649 Roberts, J.L., and Treagus, J.E. (1977) The Dalradian rocks of the South-west Highlands-
650 Introduction. Scottish Journal of Geology, 13, 87-99.

651 Rumble, D., and Spear, F.S. (1983) Oxygen-isotope equilibration and permeability
652 enhancement during regional metamorphism. Journal of the Geological Society, 140, 619-
653 628.

654 Schliestedt, M., and Matthews, A. (1987) Transformation of blueschist to greenschist facies
655 rocks as a consequence of fluid infiltration, Sifnos (Cyclades), Greece. Contributions to
656 Mineralogy and Petrology, 97, 237-250.

657 Schumacher, J.C., Brady, J.B., Cheney, J.T., and Tonnsen, R.R. (2008) Glaucophane-bearing
658 marbles on Syros, Greece. Journal of Petrology, 49, 1667-1686.

659 Selverstone, J., Morteani, G., and Staude, J.-M. (1991) Fluid channelling during ductile
660 shearing: transformation of granodiorite into aluminous schist in the Tauern Window, Eastern
661 Alps. Journal of Metamorphic Geology, 9, 419-431.

662 Sibson, R.H., Robert, F., and Poulsen, H.K. (1988) High-angle reverse faults, fluid-pressure
663 cycling, and mesothermal gold-quartz deposits. Geology, 16, 551-555.

664 Skelton, A.D.L., Graham, C.M., and Bickle, M.J. (1995) Lithological and structural controls
665 on regional 3-D fluid flow patterns during greenschist facies metamorphism of the Dalradian
666 of the SW Scottish Highlands. Journal of Petrology, 36, 563-586.

667 Skelton, A.D.L., Bickle, M.J., and Graham, C.M. (1997) Fluid-flux and reaction rate from
668 advective-diffusive carbonation of mafic sill margins in the Dalradian, southwest Scottish
669 Highlands. Earth and Planetary Science Letters, 146, 527-539.

670 Skelton, A.D.L., Whitmarsh, R., Arghe, F., Crill, P., and Koyi, H. (2005) Constraining the
671 rate and extent of mantle serpentinization from seismic and petrological data: implications for
672 chemosynthesis and tectonic processes. Geofluids, 5, 153-164.

673 Spear, F.S. (1993) Metamorphic phase equilibria and pressure-temperature-time paths.

674 Spencer Jr., J.W. (1981) Stress relaxations at low frequencies in fluid-saturated rocks:
675 attenuation and modulus dispersion. Journal of Geophysical Research, 86, 1803-1812.

676 Thompson, A.B., and Connolly, J.A.D. (1992) Migration of metamorphic fluid: some aspects
677 of mass and heat transfer. Earth-Science Reviews, 32, 107-121.

678 Van der Plas, L., and Tobi, A.C. (1965) A chart for judging the reliability of point counting
679 results. American Journal of Science, 263, 87-90.

Watson, B.E., and Brenan, J.M. (1987) Fluids in the lithosphere, 1. Experimentally-determined wetting characteristics of CO_2-H_2O fluids and their implications for fluid transport, host-rock physical properties, and fluid inclusion formation. Earth and Planetary Science Letters, 85, 497-515.

Whitney, D.L. and Evans, W. (2010) Abbreviations for names of rock-forming minerals. American Mineralogist, 95, 185-187.

Vorhies, S.H., and Ague, J.J. (2011) Pressure–temperature evolution and thermal regimes in the Barrovian zones, Scotland. Journal of the Geological Society, 168, 1147-1166.

Yardley, B.W.D., Gleeson, S., Bruce, S., and Banks, D. (2000) Origin of retrograde fluids in metamorphic rocks. Journal of Geochemical Exploration, 69, 281-285.

Figure captions

Figure 1. Geological map of the SW Scottish Highlands showing lithostratigraphy, metamorphic grade and major structures (modified after Roberts 1974). The small inset shows a cross-section of the regional structure of the Dalradian. IS = Islay Anticline; LAS = Loch Awe Syncline; AA = Ardrishaig Anticline; TS = Tayvallich Syncline; KBS = Kilmory Bay Syncline.

Figure 2. Locality map of Loch Stornoway showing the location of the sampled profile and location of samples for microprobe analyses. Photomicrographs (in plane polarized light) showing progressive pseudomorphic replacement of garnet by chlorite along the profile. (a) Fully replaced garnet in the foliated part of the sill margin. (b) Partly replaced garnet in unfoliated part of the sill margin. (c) and (d) Partly replaced garnet in the unfoliated part of the sill interior. (e) Preserved garnets in the unfoliated part of the sill interior. (f) Preserved garnets in foliated part of the sill interior.

Figure 3. Point-counting data along the profile for amphibole, quartz, biotite, albite, epidote, chlorite and carbonates. Gray shaded areas indicate parts of the sill that are foliated.

Figure 4. Photomicrographs (in plane and cross polarized light) showing the appearance of amphibole (a) in the sill interior and (b) in the sill margin. (c) Patchy appearance of calcite overgrowing the foliation in the sill margins. amp = amphibole; cal = calcite; ep = epidote; grt = garnet; qz = quartz (mineral abbreviations after Whitney and Evans 2010).

Figure 5. Photomicrographs (in plane and cross polarized light) showing reaction textures caused by carbonation. (a) Replacement of amphibole by calcite and chlorite. (b) Replacement of epidote by calcite. (c) Replacement of biotite by calcite and chlorite. (d) Replacement of garnet by chlorite and calcite. amp = amphibole; bt = biotite; cal = calcite; chl = chlorite; ep = epidote; qz = quartz (mineral abbreviations after Whitney and Evans 2010).

Figure 6. Photomicrographs (in plane and cross polarized light) showing textures of epidote and garnet. (a) Common appearance of epidote in the metabasaltic sills. (b) Replacement of garnet by epidote and chlorite. (c) Preserved garnet close to the sill margin enclosed by coarse-grained quartz and a partially replaced garnet surrounded by hydrous minerals such as amphibole. (d) Preserved garnet from the sill margins which is enclosed completely by calcite. amp = amphibole; cal = calcite; chl = chlorite; ep = epidote; grt = garnet; qz = quartz (mineral abbreviations after Whitney and Evans 2010).

Figure 7. (a) Abundance of preserved and partially replaced garnet across the metabasaltic sill. (b) Averaged degrees of replacement of garnets from samples along the profile with 1.0 = fully replaced garnet, 0.5 = partially replaced garnet and 0.0 = preserved garnet. White diamonds indicate that in these samples garnet was replaced by chlorite and calcite while black diamonds indicate replacement of garnet only by chlorite ± epidote. (c) Variation of the

726 averaged size of garnet grains along the profile. Gray shaded areas indicate parts of the sill
727 that are foliated.

728 Figure 8. SEM backscattered (BSE) and second electron (SE) images showing (a) the porosity
729 of newly formed chlorite and crack opening of garnet due to an interface-coupled dissolution-
730 precipitation mechanism during hydration reaction. White arrows indicate areas of high
731 porosity and crack opening. (b) Finger-like replacement of amphibole by calcite. Thereby,
732 calcite grows along cleavage planes of the amphibole. amp = amphibole; cal = calcite; chl =
733 chlorite; grt = garnet (mineral abbreviations after Whitney and Evans 2010).

734 Figure 9. Profile across the Loch Stornoway sills showing whole rock chemistry. Gray shaded
735 areas indicate parts of the sill that are foliated.

736 Figure 10. The abundance of biotite plotted against the concentration of K_2O in the
737 metabasaltic sill. This figure shows a positive correlation between the abundance of biotite
738 and concentration of K which implies that biotite formation is controlled by the availability of
739 K.

740 Figure 11. T-X_{CO2} diagrams showing reactions (1), (2) and (3). Dashed lines indicate that the
741 reactions are metastable at these T-X_{CO2} conditions. (a) Illustration of reaction pathway 1
742 where infiltration of an externally-buffered fluid occurred down temperature (blue arrow). (b)
743 Infiltration of a fluid with X_{CO2} = 0.002 – 0.003 at a given temperature range of 290 to 400°C
744 (from garnet-chlorite geothermometry, red box) will simultaneously drive reactions 2 and 3
745 (reaction pathway 2). This is possible as the X_{CO2} of the infiltrating fluid is greater than that
746 which is buffered by reaction 3 and less than that which is buffered by the reaction 2. alm =
747 almandine; cal = calcite; czo = clinozoisite; dph = daphnite; fac = ferroactinolite; qz = quartz
748 (mineral abbreviations after Whitney and Evans 2010).

749 Figure 12. Schematic sketch of the sequence of events as indicated from the sills in this study
750 are development of foliation during prograde to peak metamorphism on the margins of the
751 sills and was contemporaneous with garnet growth. Infiltration of H_2O-CO_2 fluid occurred
752 after peak metamorphism.

753 Table 1. Mineral modes (in vol%) along a profile across one of the sills at Loch Stornoway.

754 Table 2. Representative mineral compositions and their corresponding molar volumes and
755 densities from samples of the group of sills at Loch Stornoway.

756 Table 3. Comparisons of the garnet-amphibole geothermometers.

757 Table 4. Comparisons of the garnet-chlorite geothermometers.

758 Table 5. Whole rock chemistry (in wt%) along a profile across one of the sills at Loch
759 Stornoway.

760

Figure 1

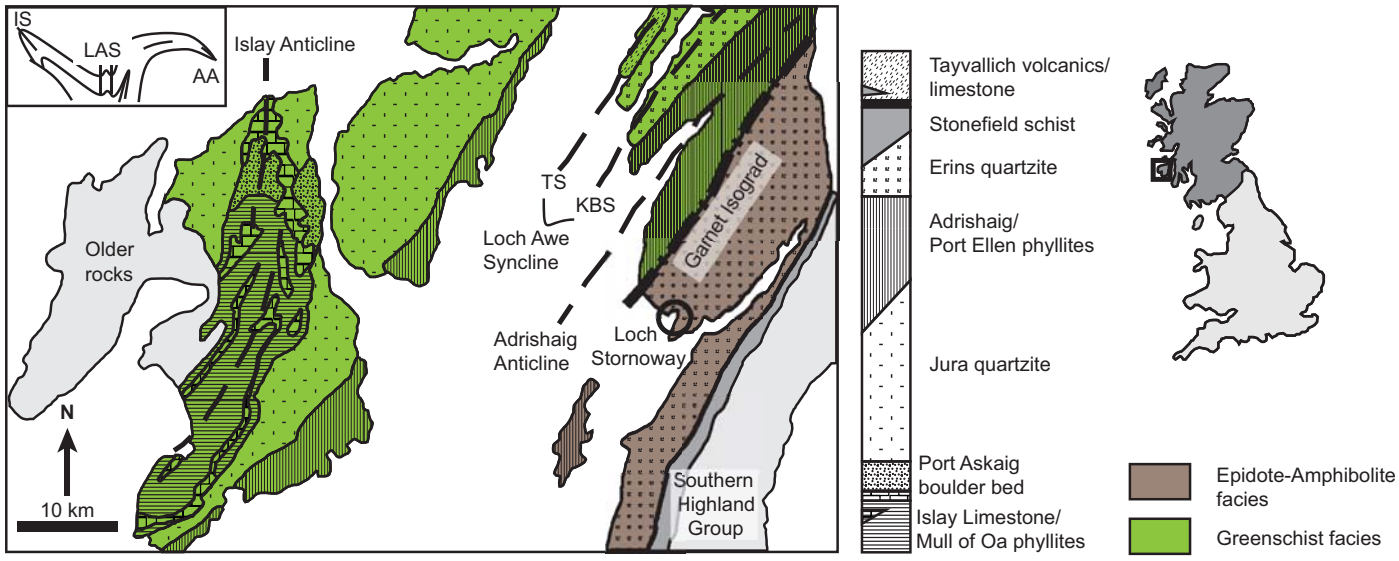
IS
LAS
AA
Islay Anticline
Older rocks
TS
KBS
Loch Awe Syncline
Garnet Isograd
Adrishaig Anticline
Loch Stornoway
Southern Highland Group
N
10 km
Tayvallich volcanics/ limestone
Stonefield schist
Erins quartzite
Adrishaig/ Port Ellen phyllites
Jura quartzite
Port Askaig boulder bed
Islay Limestone/ Mull of Oa phyllites
Epidote-Amphibolite facies
Greenschist facies

Figure 2

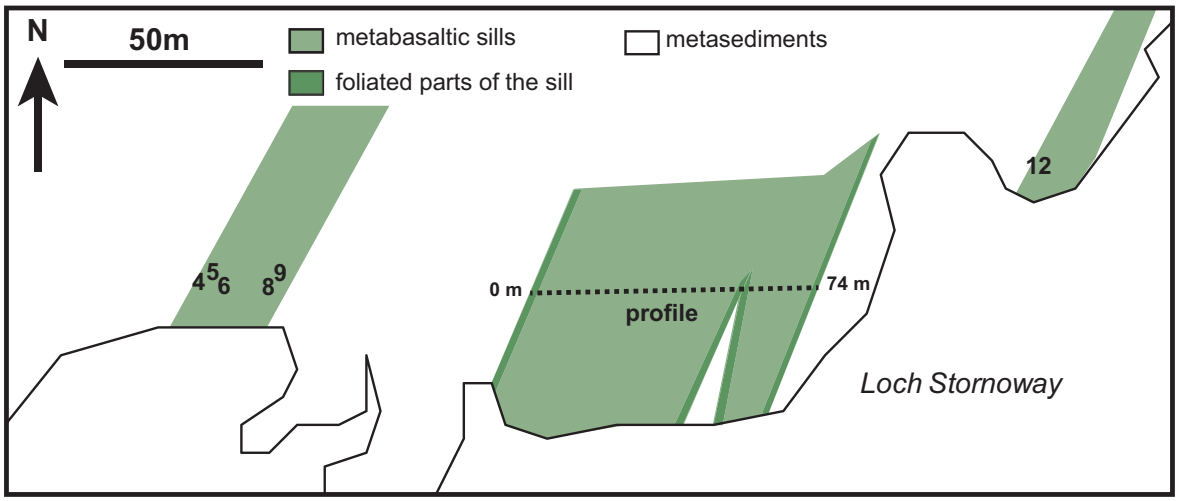
N
50m
metabasaltic sills
foliated parts of the sill
metasediments
4 5 6 8 9
12
0 m
74 m
profile
Loch Stornoway

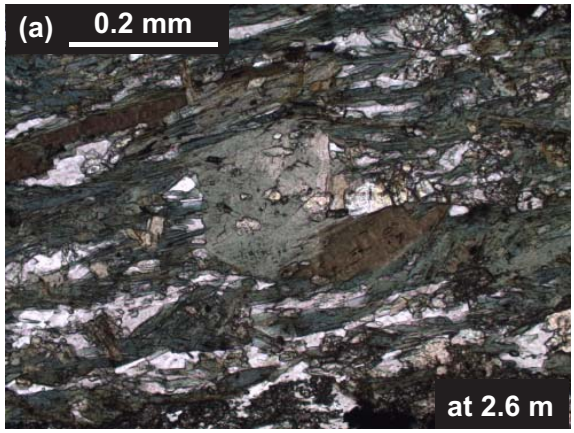
(a)
0.2 mm
at 2.6 m

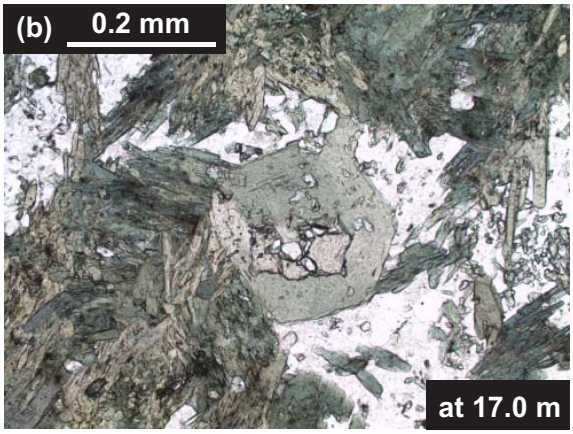
(b)
0.2 mm
at 17.0 m

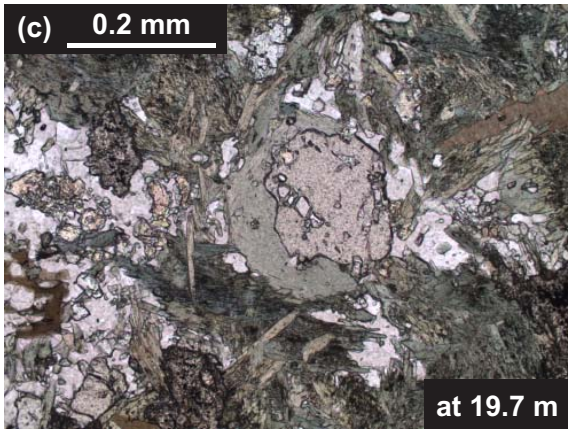
(c)
0.2 mm
at 19.7 m

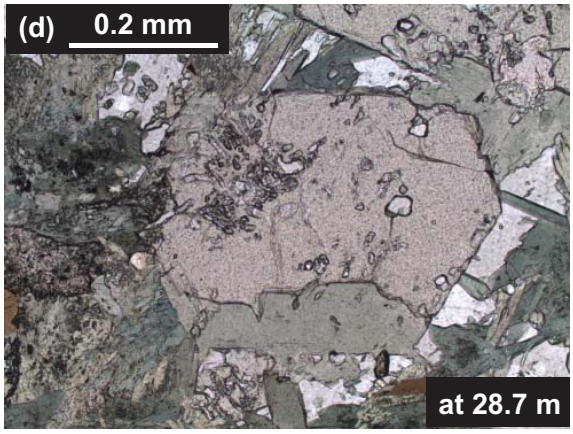
(d)
0.2 mm
at 28.7 m

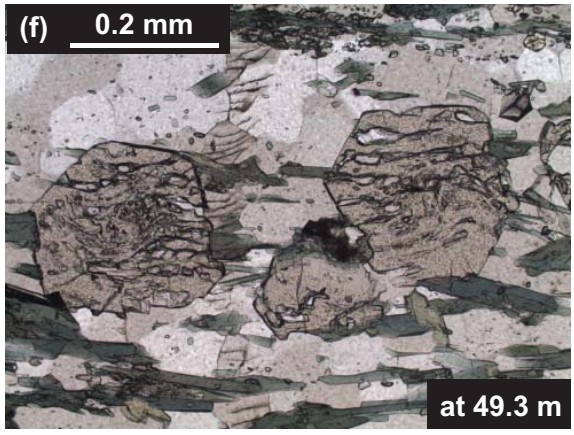
(f)
0.2 mm
at 49.3 m

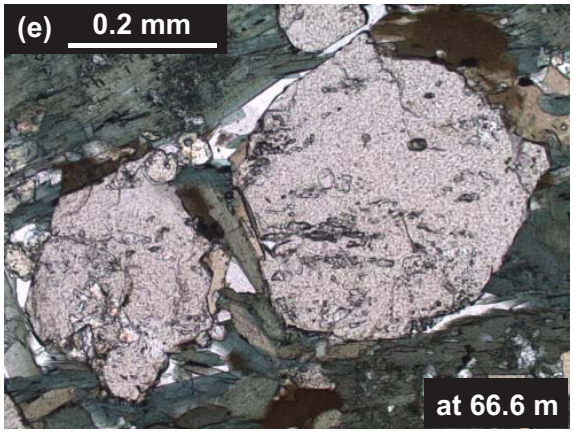
(e)
0.2 mm
at 66.6 m

Figure 3

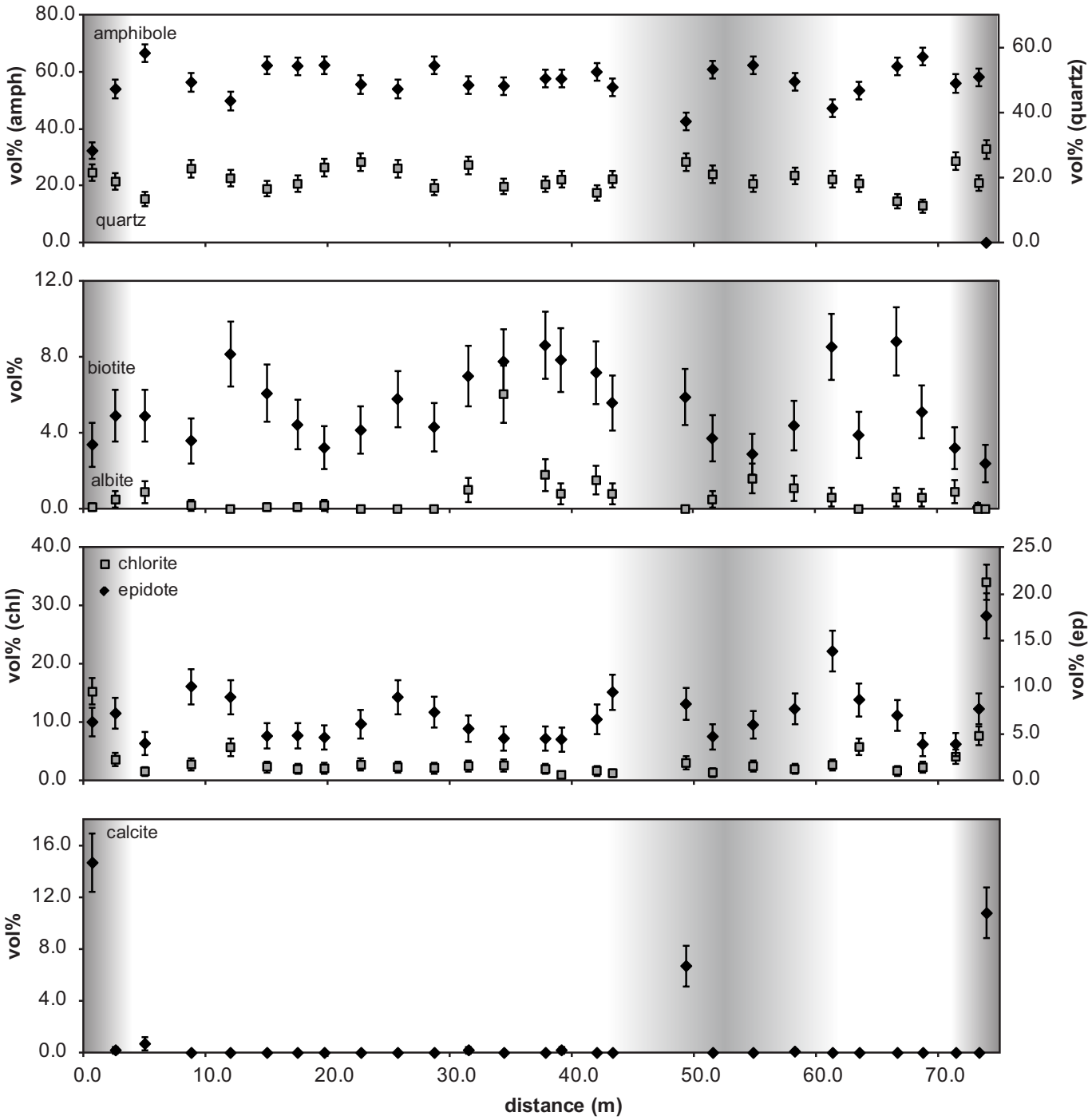
amphibole
quartz
vol% (amph)
vol% (quartz)
biotite
albite
vol%
chlorite
epidote
vol% (chl)
vol% (ep)
calcite
distance (m)

Figure 4

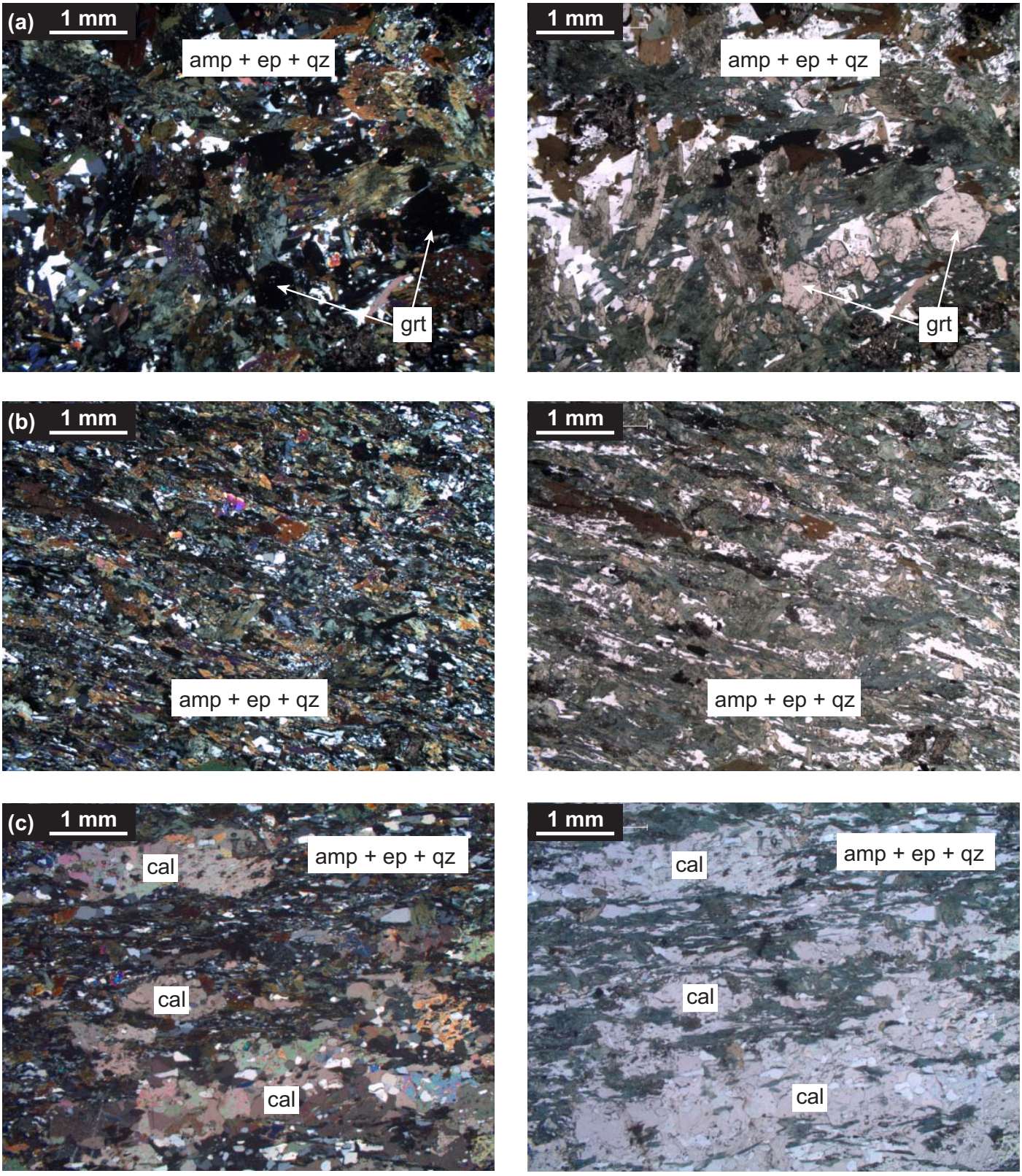
(a)
1 mm
amp + ep + qz
grt
1 mm
amp + ep + qz
grt
(b)
1 mm
amp + ep + qz
1 mm
amp + ep + qz
(c)
1 mm
cal
amp + ep + qz
cal
cal
1 mm
cal
amp + ep + qz
cal
cal

Figure 5

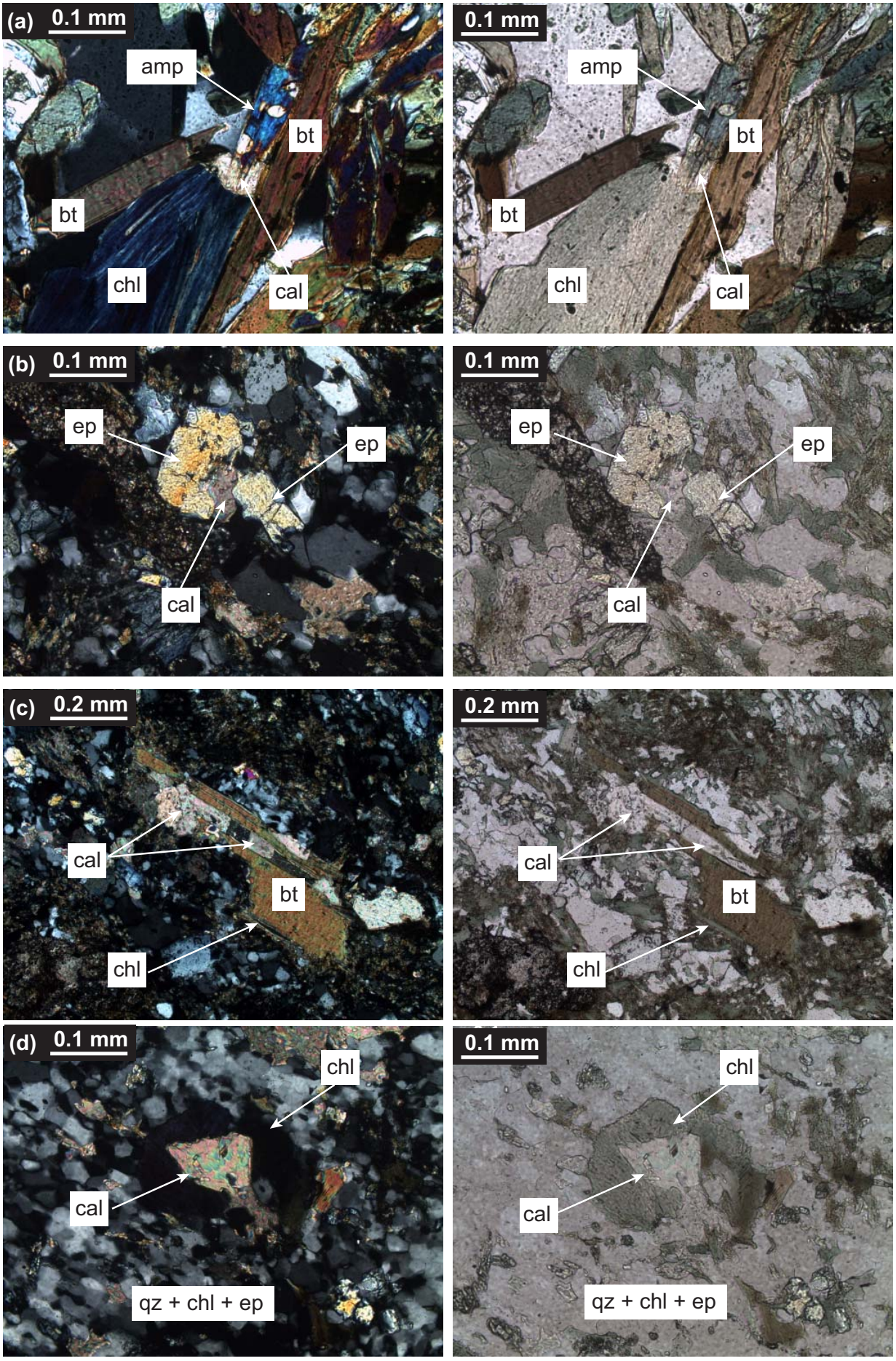
(a)
0.1 mm
amp
bt
bt
chl
cal
0.1 mm
amp
bt
bt
chl
cal
(b)
0.1 mm
ep
ep
cal
0.1 mm
ep
ep
cal
(c)
0.2 mm
cal
bt
chl
0.2 mm
cal
bt
chl
(d)
0.1 mm
chl
cal
qz + chl + ep
0.1 mm
chl
cal
qz + chl + ep

Figure 6

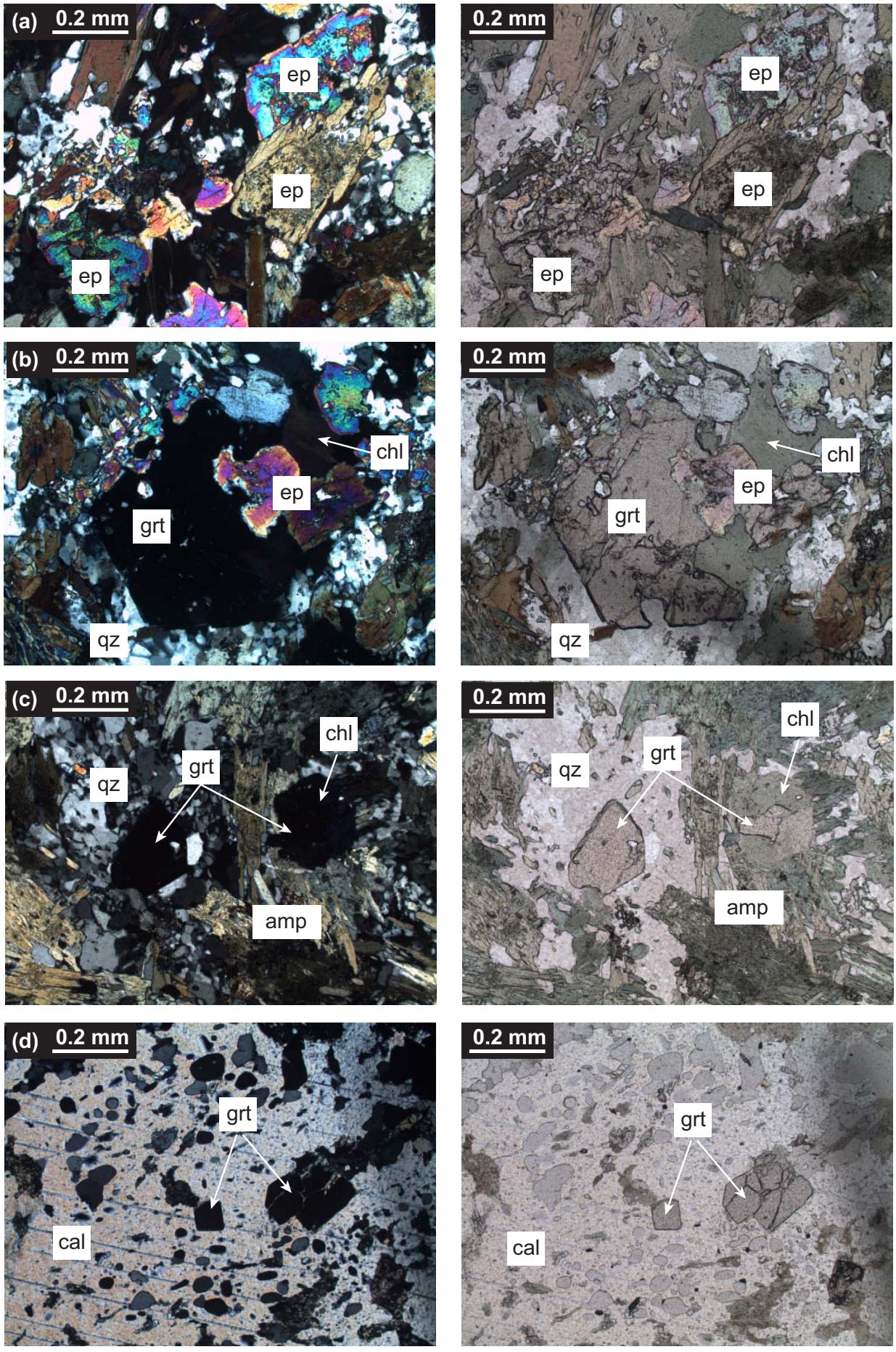
(a)
0.2 mm
ep
ep
ep
0.2 mm
ep
ep
ep
(b)
0.2 mm
chl
ep
grt
qz
0.2 mm
chl
ep
grt
qz
(c)
0.2 mm
chl
qz
grt
amp
0.2 mm
chl
qz
grt
amp
(d)
0.2 mm
grt
cal
0.2 mm
grt
cal

Figure 7

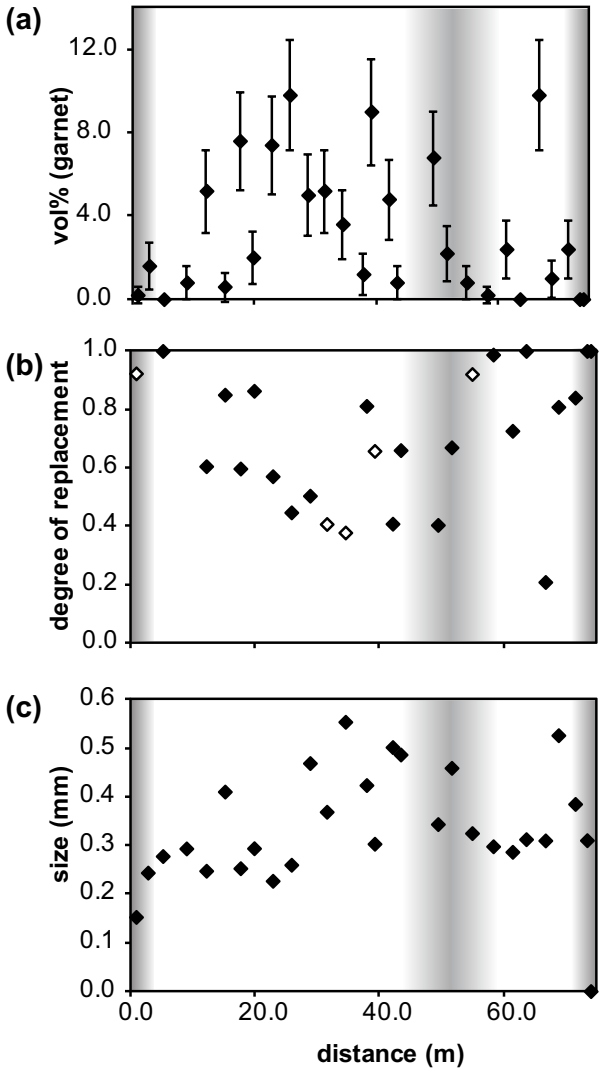
(a)
vol% (garnet)
12.0
8.0
4.0
0.0
(b)
degree of replacement
1.0
0.8
0.6
0.4
0.2
0.0
(c)
size (mm)
0.6
0.5
0.4
0.3
0.2
0.1
0.0
0.0
20.0
40.0
60.0
distance (m)

Figure 8

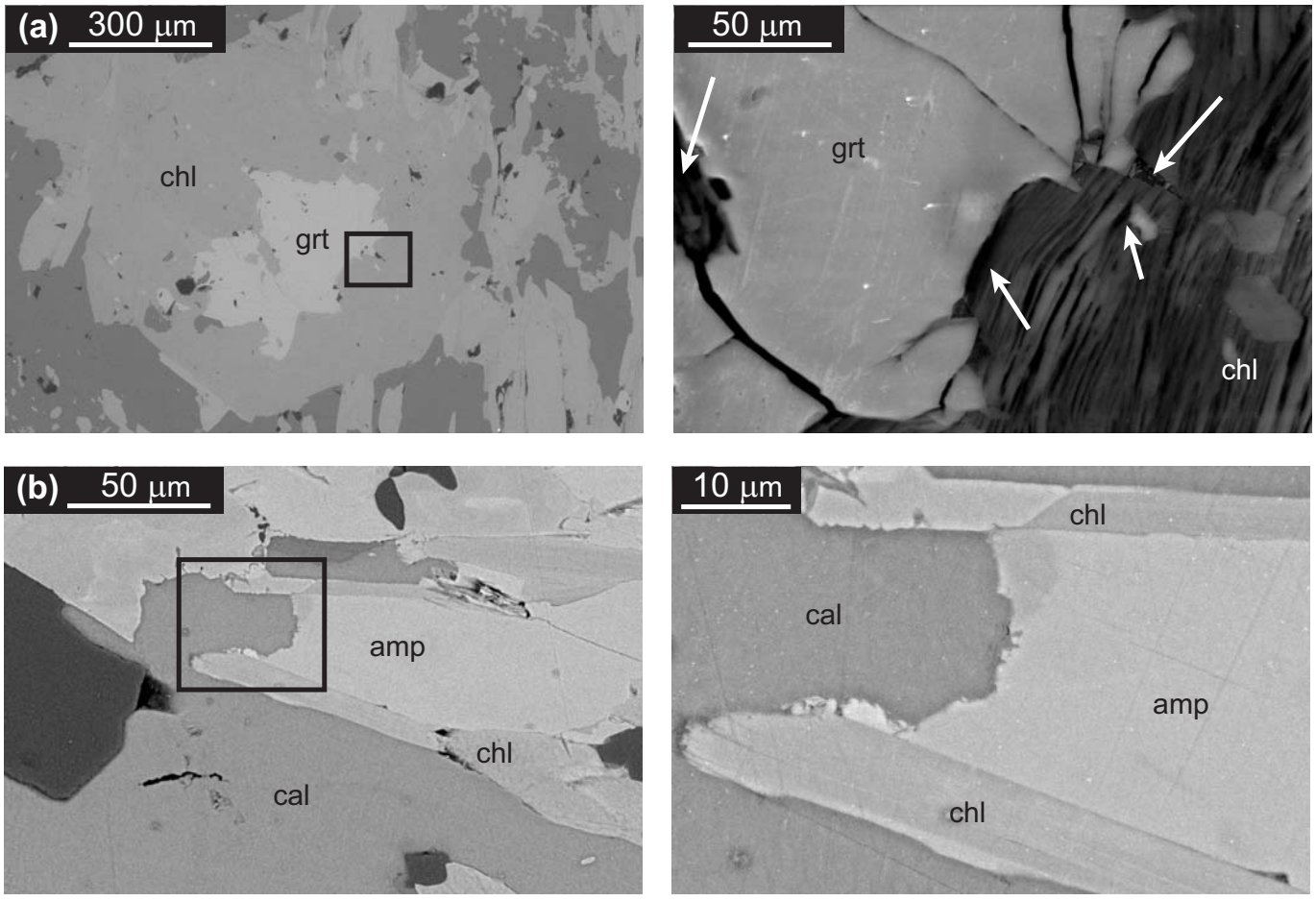
(a)
300 μm
chl
grt
50 μm
grt
chl
(b)
50 μm
amp
chl
cal
10 μm
chl
cal
amp
chl

Figure 9

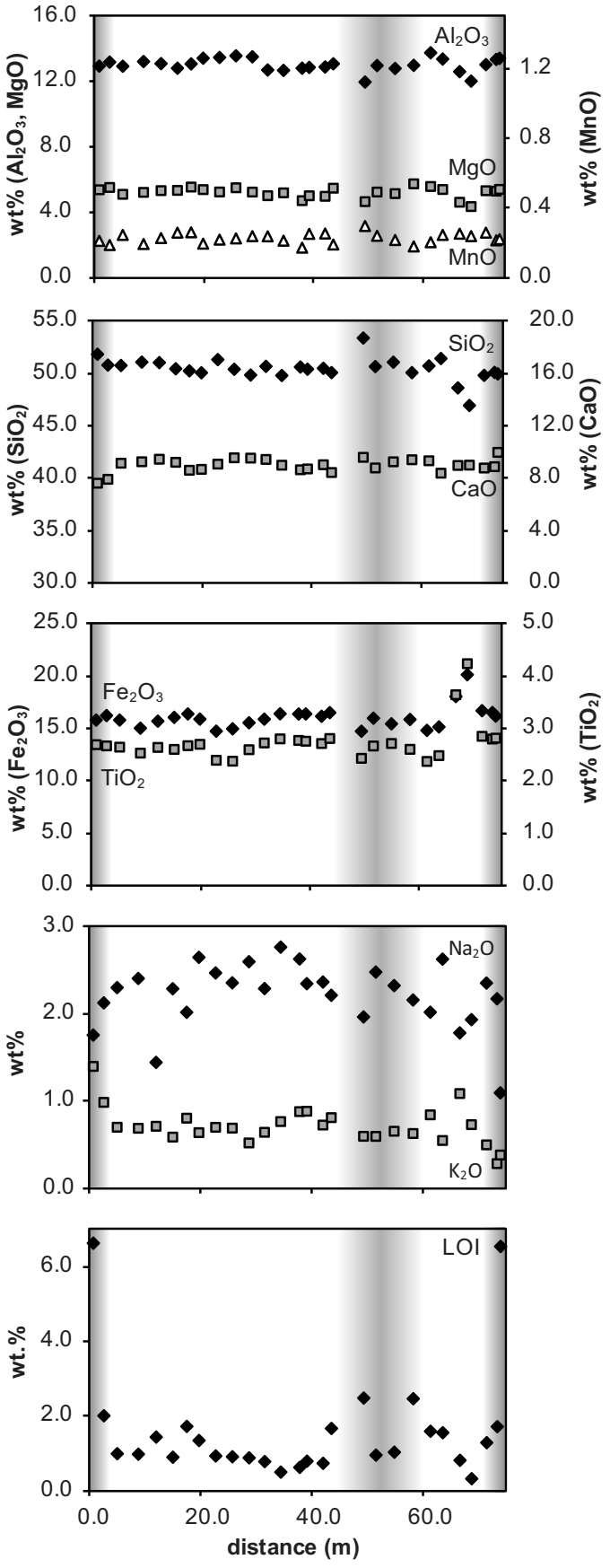
Al2O3
MgO
MnO
wt% (Al2O3, MgO)
wt% (MnO)
SiO2
CaO
wt% (SiO2)
wt% (CaO)
Fe2O3
TiO2
wt% (Fe2O3)
wt% (TiO2)
Na2O
K2O
wt%
LOI
wt.%
distance (m)

Figure 10

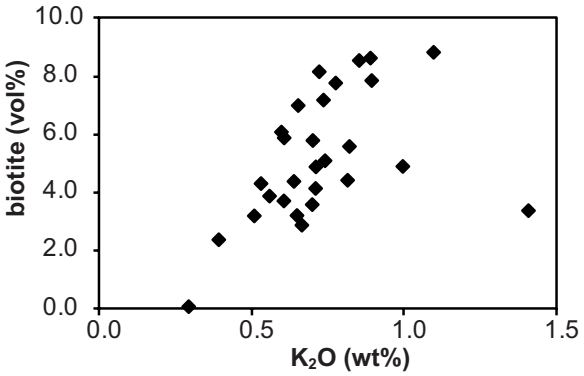

Figure 11

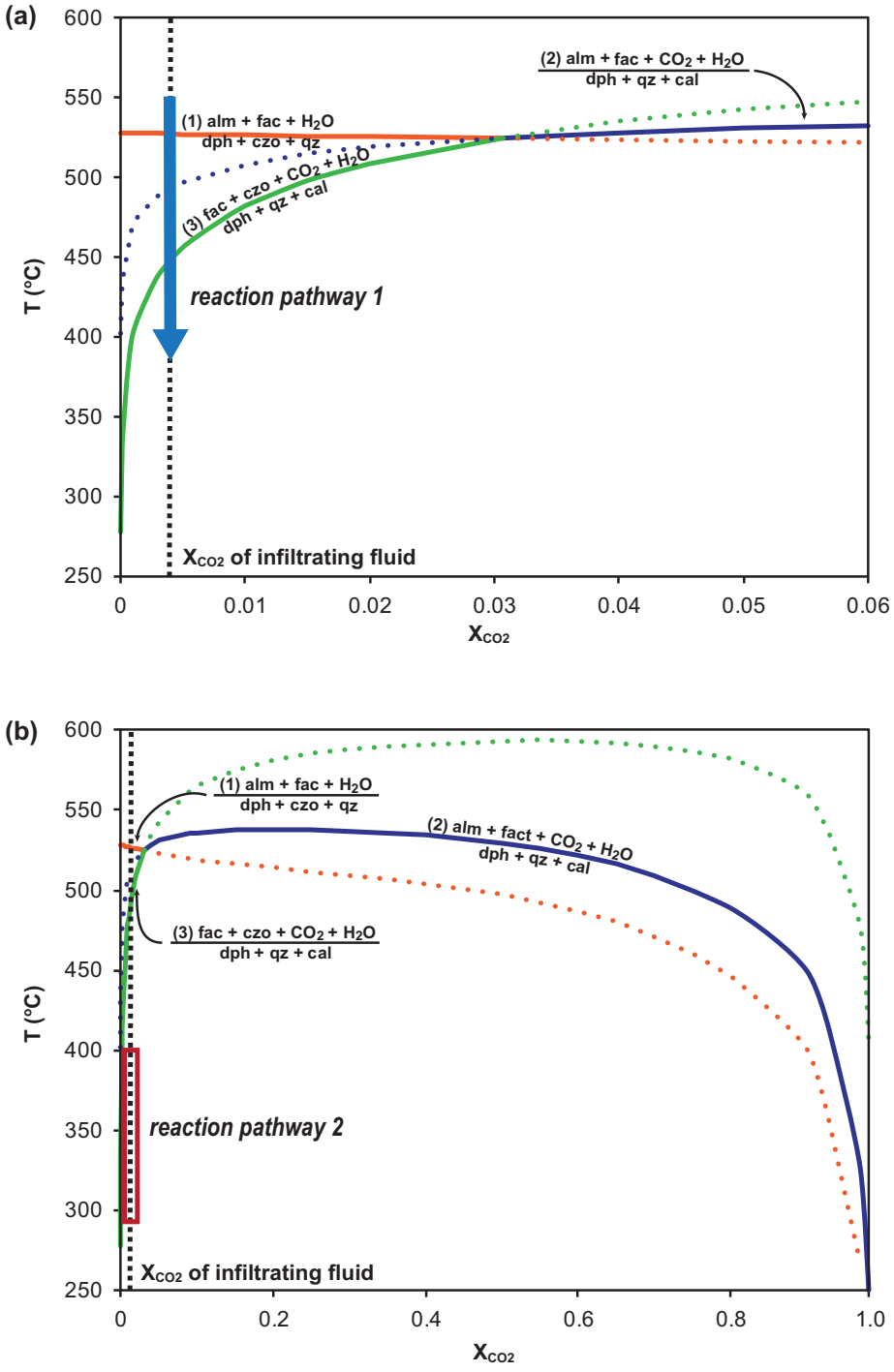
(a)
600
550
500
450
400
350
300
250
T (°C)
0
0.01
0.02
0.03
0.04
0.05
0.06
X_{CO2}
(1) alm + fac + H_2O
dph + czo + qz
(2) alm + fac + CO_2 + H_2O
dph + qz + cal
(3) fac + czo + CO_2 + H_2O
dph + qz + cal
reaction pathway 1
X_{CO2} of infiltrating fluid
(b)
600
550
500
450
400
350
300
250
T (°C)
0
0.2
0.4
0.6
0.8
1.0
X_{CO2}
(1) alm + fac + H_2O
dph + czo + qz
(2) alm + fact + CO_2 + H_2O
dph + qz + cal
(3) fac + czo + CO_2 + H_2O
dph + qz + cal
reaction pathway 2
X_{CO2} of infiltrating fluid

Figure 12

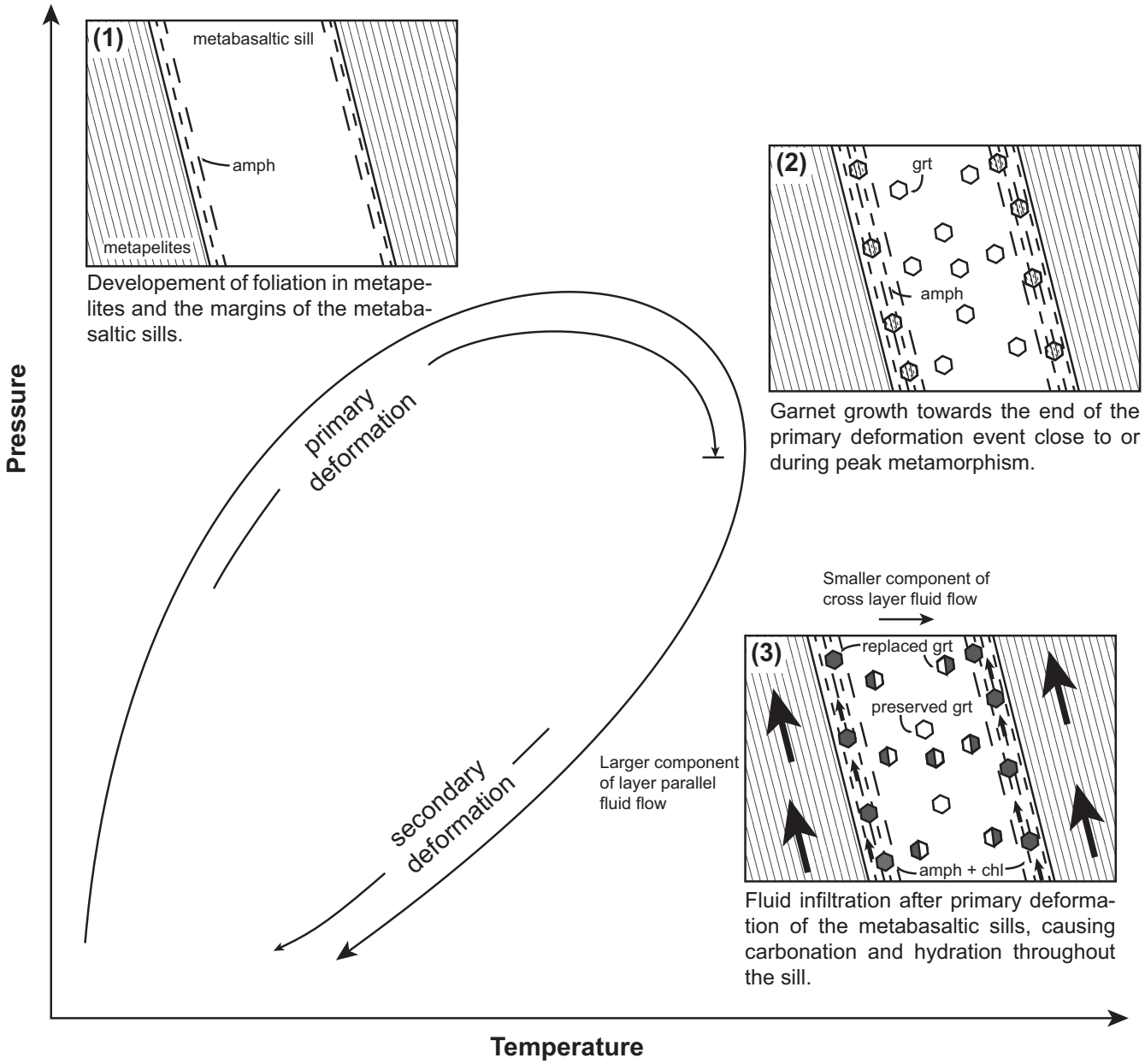
(1)
metabasaltic sill
amph
metapelites
Developement of foliation in metapelites and the margins of the metabasaltic sills.
(2)
grt
amph
Garnet growth towards the end of the primary deformation event close to or during peak metamorphism.
Pressure
primary deformation
secondary deformation
Larger component of layer parallel fluid flow
Smaller component of cross layer fluid flow
(3)
replaced grt
preserved grt
amph + chl
Fluid infiltration after primary deformation of the metabasaltic sills, causing carbonation and hydration throughout the sill.
Temperature

Table 1. Mineral modes (in vol%) along a profile across one of the sills at Loch Stornoway.

sample	**LS-0.7**		**LS-2.6**		**LS-5.0**		**LS-8.8**		**LS-12.0**		**LS-15.0**		**LS-17.5**		**LS-19.7**		**LS-22.7**		**LS-25.7**	
distance (m)	**0.7**		**2.6**		**5.0**		**8.8**		**12.0**		**15.0**		**17.5**		**19.7**		**22.7**		**25.7**	
biotite	3.4	± 1.1	4.9	± 1.4	4.9	± 1.4	3.6	± 1.2	8.2	± 1.7	6.1	± 1.5	4.4	± 1.3	3.2	± 1.1	4.2	± 1.3	5.8	± 1.5
amphibole	32.4	± 3.0	54.1	± 3.2	66.8	± 3.0	56.5	± 3.1	49.9	± 3.2	62.4	± 3.1	62.2	± 3.1	62.5	± 3.1	55.7	± 3.1	54.1	± 3.2
epidote	6.3	± 1.5	7.2	± 1.6	4.0	± 1.2	10.1	± 1.9	9.0	± 1.8	4.8	± 1.4	4.8	± 1.4	4.6	± 1.3	6.1	± 1.5	9.0	± 1.8
albite	0.1	± 0.2	0.5	± 0.4	0.9	± 0.6	0.2	± 0.3	0.0	± 0	0.1	± 0.1	0.1	± 0.1	0.2	± 0.3	0.0	± 0	0.0	± 0
titanite	6.0	± 1.5	9.8	± 1.9	6.7	± 1.6	3.8	± 1.2	7.2	± 1.6	7.3	± 1.6	7.8	± 1.7	3.9	± 1.2	6.3	± 1.5	5.7	± 1.5
rutile	0.0	± 0	0.0	± 0	0.0	± 0	0.0	± 0	0.0	± 0	0.0	± 0	0.2	± 0.2	0.0	± 0	0.1	± 0.1	0.1	± 0.2
chlorite	15.3	± 2.3	3.6	± 1.2	1.6	± 0.8	2.8	± 1.0	5.8	± 1.5	2.4	± 1.0	2.0	± 0.9	2.1	± 0.9	2.7	± 1.0	2.3	± 1.0
calcite	14.7	± 2.2	0.2	± 0.3	0.7	± 0.5	0.0	± 0	0.0	± 0	0.0	± 0	0.0	± 0	0.0	± 0	0.0	± 0	0.0	± 0
quartz	21.6	± 2.6	18.9	± 2.5	13.5	± 2.2	22.8	± 2.7	19.9	± 2.5	16.6	± 2.4	18.2	± 2.4	23.2	± 2.7	24.9	± 2.7	22.9	± 2.7
Fe-oxides	0.2	± 0.3	0.7	± 0.5	0.9	± 0.6	0.1	± 0.1	0.1	± 0.1	0.3	± 0.3	0.2	± 0.3	0.1	± 0.1	0.0	± 0	0.0	± 0

Errors were calculated by using the statistical approach of Van der Plas and Tobi (1965).

Table 1. continued.

sample	**LS-28.7**		**LS-31.5**		**LS-34.4**		**LS-37.8**		**LS-39.1**		**LS-42.0**		**LS-43.5**		**LS-49.3**		**LS-51.5**	
distance (m)	**28.7**		**31.5**		**34.4**		**37.8**		**39.1**		**42.0**		**43.3**		**49.3**		**51.5**	
biotite	4.3	± 1.3	7.0	± 1.6	7.8	± 1.7	8.6	± 1.8	7.9	± 1.7	7.2	± 1.6	5.6	± 1.5	5.9	± 1.5	3.7	± 1.2
amphibole	62.3	± 3.1	55.5	± 3.1	55.2	± 3.1	57.8	± 3.1	57.7	± 3.1	60.1	± 3.1	54.8	± 3.1	42.7	± 3.1	61.0	± 3.1
epidote	7.4	± 1.7	5.6	± 1.5	4.6	± 1.3	4.5	± 1.3	4.4	± 1.3	6.6	± 1.6	9.5	± 1.9	8.2	± 1.7	4.7	± 1.3
albite	0.0	± 0	1.0	± 0.6	6.1	± 1.5	1.8	± 0.8	0.8	± 0.6	1.5	± 0.8	0.8	± 0.6	0.0	± 0	0.5	± 0.4
titanite	6.3	± 1.5	3.8	± 1.2	5.5	± 1.4	6.4	± 1.6	7.9	± 1.7	6.3	± 1.5	8.1	± 1.7	7.3	± 1.6	6.3	± 1.5
rutile	0.3	± 0.3	0.0	± 0	0.1	± 0.2	0.1	± 0.2	0.0	± 0	0.0	± 0	0.1	± 0.1	0.0	± 0	0.4	± 0.4
chlorite	2.2	± 0.9	2.5	± 1.1	2.6	± 1.0	2.0	± 0.9	1.0	± 0.6	1.7	± 0.8	1.3	± 0.7	3.1	± 1.1	1.4	± 0.7
calcite	0.0	± 0	0.2	± 0.3	0.0	± 0	0.0	± 0	0.2	± 0.2	0.0	± 0	0.0	± 0	6.7	± 1.6	0.0	± 0
quartz	16.9	± 2.4	24.0	± 2.7	17.3	± 2.4	18.0	± 2.4	19.5	± 2.5	15.4	± 2.3	19.6	± 2.5	24.9	± 2.7	21.1	± 2.6
Fe-oxides	0.2	± 0.3	0.4	± 0.4	0.9	± 0.6	0.7	± 0.5	0.6	± 0.5	1.1	± 0.7	0.2	± 0.3	1.1	± 0.7	0.8	± 0.6

Errors were calculated by using the statistical approach of Van der Plas and Tobi (1965).

Table 1. continued.

sample	**LS-54.8**		**LS-58.2**		**LS-61.3**		**LS-63.5**		**LS-66.6**		**LS-68.7**		**LS-71.4**		**LS-73.3**		**LS-73.9**	
distance (m)	**54.8**		**58.2**		**61.3**		**63.5**		**66.6**		**68.7**		**71.4**		**73.3**		**73.9**	
biotite	2.9	± 1.1	4.4	± 1.3	8.6	± 1.8	3.9	± 1.2	8.8	± 1.8	5.1	± 1.4	3.2	± 1.1	0.1	± 0.1	2.4	± 1.0
amphibole	62.5	± 3.1	56.8	± 3.1	47.3	± 3.2	53.6	± 3.2	62.1	± 3.1	65.5	± 3.0	56.1	± 3.1	58.4	± 3.1	0.0	± 0
epidote	6.0	± 1.5	7.7	± 1.7	13.9	± 2.2	8.7	± 1.8	7.0	± 1.6	3.9	± 1.2	3.9	± 1.2	7.7	± 1.7	17.7	± 2.4
albite	1.6	± 0.8	1.1	± 0.7	0.6	± 0.5	0.0	± 0	0.6	± 0.5	0.6	± 0.5	0.9	± 0.6	0.0	± 0	0.0	± 0
titanite	5.8	± 1.5	7.1	± 1.6	7.3	± 1.6	9.4	± 1.8	5.5	± 1.4	7.2	± 1.6	5.2	± 1.4	7.1	± 1.6	4.0	± 1.2
rutile	0.1	± 0.2	0.0	± 0	0.0	± 0	0.1	± 0.1	0.1	± 0.1	0.0	± 0	0.0	± 0	0.0	± 0	0.0	± 0
chlorite	2.5	± 1.0	2.0	± 0.9	2.7	± 1.0	5.8	± 1.5	1.7	± 0.8	2.3	± 1.0	4.1	± 1.3	7.7	± 1.7	34.1	± 3.0
calcite	0.0	± 0	0.1	± 0.1	0.0	± 0	0.0	± 0	0.0	± 0	0.0	± 0	0.0	± 0	0.0	± 0	10.8	± 2.0
quartz	18.2	± 2.4	20.7	± 2.6	19.5	± 2.5	18.3	± 2.4	12.8	± 2.1	11.4	± 2.0	25.2	± 2.7	18.4	± 2.5	28.9	± 2.9
Fe-oxides	0.4	± 0.4	0.1	± 0.2	0.1	± 0.2	0.2	± 0.2	1.3	± 0.7	3.9	± 1.2	1.3	± 0.7	0.6	± 0.5	2.1	± 0.9

Errors were calculated by using the statistical approach of Van der Plas and Tobi (1965).

Table 2. Representative mineral compositions and their corresponding molar volumes and densities from samples of the group of sills at Loch Stornoway.

Sample	**LS9**	**LS9**	**LS6**	**LS5**	**LS8**	**LS6**	**LS4**	**LS12**
Phase	**garnet**		**biotite**	**chlorite**		**amphibole**	**epidote**	**plagioclase**
Comment	**core**	**rim**	**matrix**	**in garnet**	**matrix**	**matrix**	**matrix**	**matrix**
SiO_2	37.38	37.21	36.25	25.06	25.88	46.91	38.54	68.71
TiO_2	0.20	0.11	1.87	0.07	0.07	0.30	0.15	0.03
Al_2O_3	20.55	20.56	16.26	20.89	20.38	8.77	26.65	19.09
[a]$FeO_{(tot)}$	23.46	26.59	22.34	28.61	28.11	18.23	7.72	0.12
MnO	7.30	5.55	0.19	0.22	0.17	0.31	0.17	n.d.
MgO	0.37	0.73	9.36	13.50	13.99	9.71	n.d.	n.d.
CaO	10.76	9.65	0.41	0.03	0.09	11.54	23.43	0.10
Na_2O	n.d.	n.d.	0.07	0.02	0.07	1.18	0.08	11.52
K_2O	n.d.	0.003	7.81	n.d.	n.d.	0.29	n.d.	0.09
Total	100.02	100.40	94.55	88.39	88.75	97.25	96.73	99.65
Si	3.00	2.99	3.06	2.67	2.73	7.00	3.02	3.01
Ti	0.01	0.01	0.12	0.01	0.01	0.03	0.01	0.001
Al	1.95	1.95	1.62	2.62	2.54	1.54	2.46	0.99
Fe^{3+}	-	-	-	-	-	0.19	0.51	-
Fe^{2+}	1.58	1.79	1.58	2.55	2.48	2.08	-	0.004
Mn	0.50	0.38	0.01	0.02	0.02	0.04	0.01	-
Mg	0.04	0.09	1.18	2.14	2.20	2.16	-	-
Ca	0.93	0.83	0.04	0.003	0.01	1.85	1.97	0.004
Na	-	-	0.01	0.004	0.01	0.34	0.01	0.98
K	-	< 0.001	0.84	-	-	0.06	-	0.005
X_{py}	0.01	0.03						
X_{alm}	0.52	0.58						
X_{gross}	0.30	0.27						
X_{spess}	0.16	0.12						
X_{Fe}			0.57	0.54	0.53	0.49		
X_{cz}							0.48	
X_{ab}								0.99
[b]Molar volume (cm^3/mol)	118.69	118.25	152.32	212.26	212.22	274.84	137.76	100.11

Estimated relative errors for major elements are ± 1% in all analyses.

[a]$FeO_{(tot)}$ = total iron.
[b]molar volumes were calculated by using endmember molar volumes from Holland and Powell (1998) and multiplying these values with mineral fractions of the measured minerals.

Table 3. Comparisons of the garnet-amphibole geothermometers.

	garnet-amphibole geothermometer	
Sample	**Graham & Powell 1984**	**Ravna 2000**
LS5	503.3	426.4
LS5	452.2	370.8
LS6	467.5	374.0
LS6	405.1	295.9
LS8	468.6	398.2
LS9	505.2	430.9
LS5m	402.0	299.8
LS5m	402.0	299.8
LS5m	450.5	361.0
LS5m	450.5	361.0
LS6m	414.4	326.9
LS8m	360.5	261.7
LS8m	418.9	333.0
LS9m	443.0	357.3

Table 4. Comparisons of the garnet-chlorite geothermometers.

	garnet-chlorite geothermometer					
Sample	**Dickenson & Hewitt, 1986 I**	**Dickenson & Hewitt, 1986 II**	**Dickenson & Hewitt, 1986 III**	**Ghent et al 1987**	**Grambling 1990**	**Perchuck 1989**
LS5	344.5	341.2	433.6	348.6	343.9	418.7
LS5	356.9	353.1	446.4	359.5	358.4	426.1
LS5	341.1	337.9	430.1	345.6	339.8	416.8
LS5	269.9	269.2	360.7	281.9	242.1	364.7
LS5	279.4	278.5	370.9	290.5	256.7	371.0
LS5	267.3	266.7	357.9	279.5	238.0	363.1
LS6	294.1	292.6	389.5	303.7	278.1	385.6
LS8	275.3	274.4	368.8	286.7	250.4	365.0
LS9	344.6	341.3	437.0	348.7	344.0	416.6
LS5m	277.7	276.7	367.2	288.9	254.0	373.4
LS6m	258.3	258.0	352.9	271.3	223.7	353.1
LS8m	263.2	262.7	355.8	275.7	231.6	356.9
LS9m	243.6	243.7	340.5	257.8	199.2	343.6

Table 5. Whole rock chemistry (in wt%) along a profile across one of the sills at Loch Stornoway.

sample	**LS-0.7**	**LS-2.6**	**LS-5.0**	**LS-8.8**	**LS-12.0**	**LS-15.0**	**LS-17.5**	**LS-19.7**	**LS-22.7**	**LS-25.7**	**LS-28.7**	**LS-31.5**	**LS-34.4**	**LS-37.8**
distance (m)	**0.7**	**2.6**	**5.0**	**8.8**	**12.0**	**15.0**	**17.5**	**19.7**	**22.7**	**25.7**	**28.7**	**31.5**	**34.4**	**37.8**
SiO_2	51.88	50.84	50.80	51.12	51.08	50.49	50.29	50.11	51.36	50.44	49.89	50.72	49.85	50.66
TiO_2	2.70	2.68	2.65	2.54	2.65	2.61	2.68	2.71	2.40	2.38	2.60	2.73	2.81	2.78
Al_2O_3	12.98	13.22	12.97	13.25	13.13	12.85	13.11	13.46	13.50	13.60	13.54	12.74	12.71	12.85
$^{a}Fe_2O_{3(tot)}$	15.85	16.28	15.84	15.07	15.74	16.10	16.43	15.93	14.79	15.01	15.59	15.93	16.44	16.42
MnO	0.22	0.19	0.25	0.20	0.23	0.26	0.26	0.20	0.22	0.23	0.24	0.24	0.22	0.18
MgO	5.42	5.56	5.14	5.26	5.37	5.38	5.58	5.43	5.28	5.54	5.28	5.05	5.23	4.75
CaO	7.65	7.95	9.18	9.29	9.48	9.25	8.64	8.71	9.11	9.59	9.57	9.47	9.02	8.68
P_2O_5	0.15	0.17	0.16	0.16	0.16	0.18	0.17	0.16	0.16	0.14	0.16	0.17	0.17	0.17
Na_2O	1.76	2.13	2.31	2.41	1.45	2.29	2.02	2.65	2.48	2.36	2.60	2.30	2.77	2.64
K_2O	1.40	0.99	0.71	0.70	0.72	0.59	0.81	0.65	0.71	0.70	0.53	0.65	0.77	0.89
LOI	6.64	2.03	1.01	1.00	1.45	0.92	1.74	1.36	0.95	0.93	0.90	0.80	0.52	0.64
CO_2	6.16	0.08	0.28	0.00	0.00	0.00	0.00	0.00	0.00	0.00	0.00	0.08	0.00	0.00
H_2O	0.48	1.95	0.73	1.00	1.45	0.92	1.74	1.36	0.95	0.93	0.90	0.72	0.52	0.64

The overall analytical error is < 5% of the measured values.

$^{a}Fe_2O_{3(tot)}$ = total iron.

Table 5. continued.

sample	**LS-39.1**	**LS-42.0**	**LS-43.5**	**LS-49.3**	**LS-51.5**	**LS-54.8**	**LS-58.2**	**LS-61.3**	**LS-63.5**	**LS-66.6**	**LS-68.7**	**LS-71.4**	**LS-73.3**	**LS-73.9**
distance (m)	**39.1**	**42.0**	**43.5**	**49.3**	**51.5**	**54.8**	**58.2**	**61.3**	**63.5**	**66.6**	**68.7**	**71.4**	**73.3**	**73.9**
SiO_2	50.45	50.53	50.12	53.42	50.70	51.12	50.12	50.76	51.47	48.66	46.99	49.86	50.14	50.00
TiO_2	2.77	2.72	2.82	2.44	2.67	2.72	2.61	2.38	2.49	3.65	4.25	2.86	2.81	2.82
Al_2O_3	12.90	12.92	13.12	12.00	13.01	12.83	13.02	13.79	13.41	12.64	12.06	13.06	13.38	13.45
$^{a}Fe_2O_{3(tot)}$	16.43	16.21	16.55	14.78	16.02	15.49	15.90	14.86	15.19	18.09	20.18	16.74	16.56	16.22
MnO	0.26	0.26	0.19	0.30	0.24	0.22	0.18	0.21	0.25	0.26	0.24	0.26	0.22	0.22
MgO	5.05	5.02	5.51	4.69	5.28	5.18	5.78	5.62	5.43	4.65	4.39	5.36	5.33	5.44
CaO	8.74	9.06	8.47	9.63	8.81	9.29	9.44	9.36	8.42	9.01	9.03	8.81	8.91	10.01
P_2O_5	0.18	0.18	0.18	0.17	0.17	0.17	0.14	0.15	0.16	0.16	0.19	0.18	0.18	0.35
Na_2O	2.35	2.37	2.22	1.97	2.49	2.33	2.17	2.03	2.63	1.79	1.94	2.36	2.18	1.10
K_2O	0.89	0.73	0.82	0.60	0.60	0.66	0.64	0.85	0.56	1.09	0.74	0.51	0.29	0.39
LOI	0.81	0.75	1.68	2.50	0.97	1.05	2.48	1.61	1.57	0.83	0.34	1.30	1.73	6.55
CO_2	0.08	0.00	0.00	2.49	0.00	0.00	0.04	0.00	0.00	0.00	0.00	0.00	0.00	4.64
H_2O	0.73	0.75	1.68	0.01	0.97	1.05	2.44	1.61	1.57	0.83	0.34	1.30	1.73	1.91

The overall analytical error is < 5% of the measured values.

$^{a}Fe_2O_{3(tot)}$ = total iron.